# Collaborative Mechanistic Effects between Vanadia and Titania during the Oxidative Dehydrogenation of Propane Investigated by Operando and Transient Spectroscopy

Leon Schumacher, Johannes Pfeiffer, Jun Shen, Torsten Gutmann, Hergen Breitzke, Gerd Buntkowsky, Kathrin Hofmann, Christian Hess*

Technical University of Darmstadt, Department of Chemistry, Eduard-Zintl-Institut für Anorganische und Physikalische Chemie, Alarich-Weiss-Str. 8, 64287 Darmstadt, Germany

*Corresponding Author (E-Mail: christian.hess@tu-darmstadt.de)

TOC
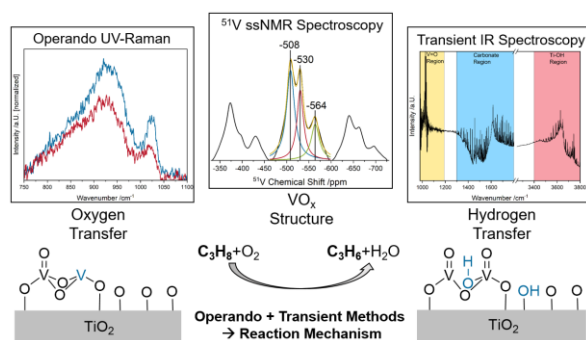
Keywords: propane ODH, vanadia, titania, transient IR spectroscopy, operando spectroscopy, nuclearity-dependence, support interaction

Abstract

The oxidative dehydrogenation (ODH) of propane is of great technical importance and supported VO_x catalysts have shown promising properties for the reaction. One of the most prominent and active supports is titania, which exhibits a high activity but many questions regarding the catalyst system are still of debate. In this study, we elucidate the mechanism of the propane ODH reaction over VO_x/TiO_2, using P25 and ALD (atomic layer deposition) synthesized TiO_2/SBA-15 as a support, with XPS, XRD, ^{51}V solid-state (ss)NMR, operando multi-wavelength Raman, operando UV-Vis, and transient IR spectroscopy. Bare titania shows a small conversion, leading to carbon formation and the reaction occurs at the interface between anatase and rutile. In comparison, in VO_x/TiO_2 catalysts the activity shifts from titania to vanadia sites. UV-Raman spectroscopy and structural characterization data revealed the reaction to involve preferentially the V=O bonds of dimeric species rather than doubly bridged V-O-V bonds, which leads to higher propene selectivities. The active vanadium site shows a nuclearity-dependent behavior, that is, at higher loadings, when oligomeric vanadia is present, it shifts from V=O bonds to linear V-O-V bonds in oligomers, leading to a less selective oxidation due to the better reducibility. Our operando/transient spectroscopic results demonstrate the direct participation of the titania support in the reaction, by influencing the degree of vanadia oligomerization and by enabling rapid hydrogen transfer from propane to vanadia via Ti-OH groups on anatase, accelerating the rate-determining step of the initial C-H bond breakage. The broader applicability of the results is confirmed by the behavior of the ALD-synthesized sample, which resembles that of P25. Our results highlight the detailed level of mechanistic understanding accessible from a multiple spectroscopic approach, which can be readily transferred to other materials and/or reactions.

1. Introduction

Propylene is an important basis chemical that is used to produce a variety of different industrial and consumer products, such as polypropylene, propylene glycol etc. The large demand for propylene by the chemical industry cannot be met by traditional production methods such as steam cracking. Therefore, the use of alternative methods of propylene production would be of great utility to close the gap between demand and supply.[1–3] One promising alternative way to produce propylene is the oxidative dehydrogenation (ODH) of propane, where, in contrast to traditional processes, oxygen is added to the feed. This has multiple advantages, including that the reaction becomes exothermic, allowing energy to be saved by heat integration of the additionally released energy. Furthermore, the reaction can occur at lower temperatures, further increasing the energy savings. Finally, the amount of coke that is traditionally formed on the catalysts during conventional processes by their oxidation to CO_x is reduced, hence increasing the catalyst lifetime and reducing waste.[1–3] The main issue in making propane ODH viable is the low selectivity of the reaction due to over-oxidation of propane to CO_x. Therefore, the reaction needs to be suitably catalyzed.

A promising class of catalysts for the reaction is supported vanadia (VO_x), which has previously been shown to be active on multiple supports (SiO_2, Al_2O_3, TiO_2, CeO_2, ZrO_2) with good selectivities.[4–8] One of the most active systems for the reaction is vanadia supported on titania (VO_x/TiO_2), which shows one of the lowest activation energies for the reaction.[4,5] The high activity has been proposed to be caused by the active participation of the support in the reaction,[3,5,6] but the elucidation of the detailed interactions within the VO_x/TiO_2 system are still a challenge. This is partly due to the strong absorption of titania in the UV range, which can lead to self-absorption of the spectroscopic signal if it is located in a similar range (e.g., UV-Raman).[9]

In previous studies, VO_x/TiO_2 catalysts were investigated for a large variety of reactions, including NH_3 selective catalytic reduction (SCR),[10–13] the combustion of volatile organic compounds (VOCs),[14,15] hydrodeoxygenation,[16] selective alcohol oxidation (methanol[17], ethanol[18]), photocatalytic reactions,[19,20] (due to the semiconducting properties of TiO_2), and also ethane[21,22] and propane ODH.[4–6,23–29] In the context of ODH reactions, a major point of discussion has been the interaction between titania and vanadia, and, in particular, the exact role of the titania support. On the one hand, this has been proposed to actively participate in the reaction via defect formation (i.e. Ti-OH or oxygen vacancy formation) and, on the other, to coordinate the

vanadium in a way that renders it more active than on other support materials.[6,30] Furthermore, the exact vanadia structure and the influence of the vanadia nuclearity on the reactivity is not clear.[13,31] The vanadyl peak for VO_x/CeO_2 shows a detailed fine structure in Raman spectra, which allows for the assignment and quantification of the distribution of vanadia nuclearities, thus determining their detailed influence on the catalytic activity.[8,32] For VO_x/TiO_2 systems, however, the situation appears to be more complex, as there are only two contributions in the vanadyl region of the Raman spectrum, which have previously been assigned to short- and long-chain vanadia species.[13,31,33] For ODH reactions over VO_x/TiO_2 previous studies have provided valuable insight into some of the aspects outlined above. For example, by use of operando X-ray absorption spectroscopy (XAS) during ethanol ODH, Zabilska et al.[18] showed that the redox cycle of the reaction takes place over vanadia rather than titania, which does not change its oxidation state. For propane ODH, despite the large number of studies on supported vanadia including VO_x/TiO_2, there are only a few operando[34] and no transient spectroscopic studies available in the literature that provide direct spectroscopic evidence of the reaction mechanism and the catalyst's mode of operation.[4–6,23–29]

In this study, we aim to provide an answer to the following key questions debated in the literature in the context of the mechanism of propane ODH over VO_x/TiO_2 catalysts: What is the active site of the catalyst and what is its nuclearity-dependence? How does the titania support influence the reaction and, more specifically, does it directly participate in the reaction? How can the selectivity behavior be explained? For that, we combine multiple experimental approaches, which have rarely been used in the context of alkane ODH before, to obtain a fresh perspective on the structural dynamics. First, we use multi-wavelength Raman spectroscopy, which has shown great potential for VO_x/CeO_2 systems, to investigate bulk titania by tuning the excitation wavelength to 385 nm. There we avoid most of the strong UV absorption of titania but can still selectively enhance the support's signal intensity due to resonance effects, allowing for the dedicated investigation of titania (385 nm) and vanadia (514 nm).[7,8] By combining this with further methods, including ^{51}V ssNMR, XPS, XRD, and operando UV-Vis as well as modulation excitation (ME-) DRIFTS (diffuse reflectance infrared Fourier transform spectroscopy), we aim to elucidate structure-activity relationships, leading to a detailed mechanistic picture. The combination of multiple operando spectroscopies and ME-DRIFTS has previously

been shown to enable an enhanced level of understanding of other oxidation catalysts.[8,35] Finally, as a reference system and to demonstrate the broader applicability of the results, we investigate the behavior of ALD-synthesized samples, which reduce the amount of bulk titania, thus minimizing the influence of UV absorption in comparison to the P25 samples with different vanadium loadings.[12,36]

2. Experimental Section

2.1. Sample Preparation

As a support, two different materials were used. Titania P25 (Aeroxide, Sigma-Aldrich, ≥99.5%) was purchased, whereas silica SBA-15 was synthesized as described previously.[37] The P25 samples were characterized by nitrogen physisorption and subsequent analysis by the Brunauer-Emmet-Teller (BET) method, yielding a surface area of 73 m²/g. They were loaded by wet-impregnation using an aqueous solution containing a 1:2 ratio of ammonium meta vanadate (AMV) and oxalic acid with four different concentrations (1.219, 0.585, 0.244, and 0.049 mol/l), resulting in samples loaded with vanadium surface densities of 2.5, 1.2, 0.5, and 0.1 V/nm², respectively, which is below monolayer loading, thus ensuring that only amorphous vanadia was present.[27] The loaded samples were dried at 120 °C for 12 h and then calcined for 4 h at 480 °C.

SBA-15 was coated with TiO_2 by ALD in a custom build set-up.[38] After 200 mg of SBA-15 have been placed in the ALD reactor, the reactor temperature was set to 60 °C (pressure: 1.3 Torr). The SBA-15 was then coated with 72 ALD cycles, where one cycle consisted of three half cycles of $TiCl_4$ and three half cycles of H_2O.[12] During each half cycle, the sample was exposed to $TiCl_4/H_2O$ for 60 s and then flushed for 60 s with nitrogen.[39] The theoretical thickness of the resulting TiO_2 thin film corresponds to 10 nm on a silicon wafer as determined by ellipsometry.[40] The coated samples were calcined in air at 600 °C for 12h to crystallize the deposited TiO_2 and will be referred to as SBA15-T (SBA-15 coated with titania). The specific surface area was determined to be 78 m²/g by using nitrogen physisorption and subsequent BET analysis. The sample was then loaded with vanadia in the same way as the P25 samples and the precursor concentration was adjusted for the different surface area, resulting in an aqueous solution with a 1:2 ratio of AMV and oxalic acid with a concentration of 0.621 mol/l, resulting in a vanadium surface density of 1.2 V/nm². A summary of the prepared samples is given in Table 1.

Table 1: Overview of the P25- and ALD-synthesized samples used in this study.

Sample Name	Surface Area /m^{2}g^{-1}	Vanadia Density /V nm^{-2}	ALD Substrate	Number of Cycles
P25	73	-	-	-
P25+0.1 V/nm²	73	0.1	-	-
P25+0.5 V/nm²	73	0.5	-	-
P25+1.2 V/nm²	73	1.2	-	-
P25+2.5 V/nm²	73	2.5	-	-
SBA15-T	78	-	SBA-15	72
SBA15-T+1.2 V/nm²	78	1.2	SBA-15	72

2.2. Catalytic Testing

Catalytic testing was performed in a CCR 1000 reaction cell (Linkam Scientific) in a fluidized bed operating mode, using 60 mg of catalyst for the P25 samples and, due to its much lower density, 25 mg of the ALD-synthesized samples. The samples were first dehydrated in 12.5% O_2/He for 1 h at 365 °C, subsequently cooled to 50 °C, exposed to 12.5% O_2/12.5% C_3H_8/He with a total flow rate of 40 ml$_n$/min, and then heated in 45 °C steps up to 550 °C, staying at each temperature for 1 h. The gas-phase composition was analyzed continuously using a gas chromatograph (GC, Agilent Technologies 7890B) equipped with a PoraPlotQ and a Molsieve column as well as a thermal conductivity detector (TCD) and a flame ionization detector (FID) in series. The set-up is connected through a twelve-way valve. One chromatogram is measured every 29 min, resulting in two chromatograms for each temperature, which were averaged. The pressure before and after the GC was monitored to correct the detected areas for pressure fluctuations. The obtained conversions were normalized to the surface area of the catalyst, due to the significantly different sample masses used for P25 and ALD-synthesized catalysts.

2.3. X-Ray Diffraction

Powder X-ray diffraction (XRD) patterns were recorded on a Stadi-P (Stoe & Cie) diffractometer with a Ge(111)-monochromator, Cu Kα_1 radiation (λ = 1.54060 Å), and

a MYTHEN-1K (Dectris) detector, using a flat sample holder in transmission geometry. The powder XRD patterns were recorded ex situ.

2.4. Diffuse Reflectance UV-Vis Spectroscopy

Diffuse reflectance (DR) UV-Vis spectra were recorded on a Jasco V-770 UV-Vis spectrometer. Dehydrated $BaSO_4$ was used as the white standard. For each experiment, 90 mg of catalyst was placed in the commercially available reaction cell (Praying Mantis High Temperature Reaction Chamber, Harrick Scientific) equipped with transparent quartz glass windows. For structural characterization, spectra were measured at room temperature after dehydration in 12.5% O_2/He for 1 h at 365 °C. Operando spectra were measured at 320 °C during reactive conditions (12.5% C_3H_8/12.5% O_2/He), and for comparison under oxidizing conditions (12.5% O_2/He), both after dehydration in 12.5% O_2/He for 1 h at 365 °C with a total flow rate of 40 ml_n/min. The spectra were further analyzed by a least-squares fitting analysis using Gaussian-Lorentzian (70/30) product functions. Product functions instead of purely Lorentzian functions were used to account for the large contribution of natural line broadening to the overall line-shape, caused by the short life-time of the electronically excited states.

2.5. UV-Raman Spectroscopy

UV-Raman spectroscopy was performed at an excitation wavelength of 385 nm generated by a laser system based on a Ti:Sa solid-state laser pumped by a frequency-doubled Nd:YAG laser (Coherent, Indigo). The fundamental wavelength is frequency doubled to 385 nm using a LiB_3O_5 crystal. The light is focused onto the sample, and the scattered light is collected by a confocal mirror setup and focused into a triple-stage spectrometer (Princeton Instruments, TriVista 555).[41] Finally, the Raman contribution is detected by a charge-coupled device (CCD, 2048 × 512 pixels) cooled to −120 °C. The spectral resolution of the spectrometer is 1 cm^{-1}. For Raman experiments, 70 mg of catalyst was placed in a CCR 1000 reactor (Linkam Scientific Instruments) equipped with a CaF_2 window (Korth Kristalle GmbH). A fluidized bed reactor was employed to avoid laser-induced changes of sample, by moving the particles in and out of the laser beam, allowing the use of a laser power of 7.5 mW at the location of the sample.

Furthermore, the fluidized bed helps to homogenize the temperature profile across the sample. Data processing included cosmic ray removal and background subtraction. For structural characterization, spectra were measured at room temperature after dehydration at 365 °C for 1 h in 12.5% O_2/He. Operando spectra were measured at 320 °C during exposure to reactive conditions (12.5% C_3H_8/12.5% O_2/He) and for comparison under oxidizing conditions (12.5% O_2/He) after 1 h of dehydration in 12.5% O_2/He at 365 °C with a total flow rate of 40 ml_n/min. The spectra were normalized by setting the value of the anatase E_g peak to one and adjusting the remaining intensity values accordingly. The spectra were further analyzed by a least-squares fitting analysis using Lorentzian functions.

2.6. Vis-Raman Spectroscopy

Visible (Vis) Raman spectroscopy was performed at 514 nm excitation, emitted from an argon ion gas laser (Melles Griot). The light was focused onto the sample, gathered by an optical fiber, and dispersed by a transmission spectrometer (Kaiser Optical, HL5R). The dispersed Raman radiation was subsequently detected by an electronically cooled CCD detector (–40 °C, 1024 × 256 pixels). The spectral resolution was 5 cm^{-1} with a wavelength stability of better than 0.5 cm^{-1}. For Raman experiments, 70 mg of catalyst was filled into a CCR 1000 reactor (Linkam Scientific Instruments) equipped with a quartz window (Linkam Scientific Instruments). A fluidized bed reactor was employed to avoid laser-induced damage, allowing the use of a laser power of 5 mW at the location of the sample. Data analysis of the Raman spectra included cosmic ray removal and an auto new dark correction as well as normalization to the anatase E_g peak. For structural characterization, spectra were measured at room temperature after dehydration in 12.5% O_2/He for 1 h at 365 °C. Operando spectra were measured at 320 °C during exposure to 12.5% C_3H_8/12.5% O_2/He, and for comparison under oxidizing conditions (12.5% O_2/He), both measured after 1 h of dehydration in 12.5% O_2/He at 365 °C with a total flow rate of 40 ml_n/min. The spectra were further analyzed by a least-squares fitting analysis using Lorentzian functions.

2.7. X-Ray Photoemission Spectroscopy

X-ray photo-electron spectroscopy (XPS) was carried out on an SSX 100 ESCA spectrometer (Surface Science Laboratories Inc.) employing a monochromatic Al Kα X-ray source (1486.6 eV) operated at 9 kV and 10 mA; the spot size was approximately 1 mm×0.25 mm. The base pressure of the analysis chamber was $<10^{-8}$ Torr. Survey spectra (eight measurements) were recorded between 0 and 1100 eV with 0.5 eV resolution, whereas detailed spectra (30 measurements) were recorded with 0.05 eV resolution. To account for sample charging, the C 1s peak of ubiquitous carbon at 284.4 eV was used to correct the binding-energy shifts in the spectra. Data analysis included a Shirley background subtraction and a peak-fit analysis using Gaussian-Lorentzian (70/30) production functions. Atomic concentrations were calculated using the relative sensitivity factors (RSFs) given in Table 2.

Table 2: Relative sensitivity factors (RSFs) used for the XPS analysis.

	C 1s	O 1s	Si 2p	Ti 2p	V 2p
RSF	0.537	2.930	0.817	7.810	9.660

2.8. Physical Characterization

The specific surface area and the pore diameter were determined by analysis of the nitrogen adsorption and desorption isotherms recorded on a Surfer BET analyzer (Thermo Fisher) after drying the samples in vacuum for 24 h. The isotherms were then analyzed by multipoint BET analysis.

2.9. ^{51}V ssNMR Spectroscopy

^{51}V ss (solid state)NMR spectra at 14.1 T were recorded on a Bruker Avance III HD 600 MHz spectrometer operating at a frequency of 157.75 MHz for ^{51}V as reported previously.[42] Experiments were performed with a 3.2 mm ^{1}H/X/Y triple resonance probe under magic angle spinning (MAS) at spinning rates of 18 and 21 kHz. Spectra were acquired using single-pulse excitation with a pulse length of 0.8 μs. This corresponds to flip-angles of ca. 30° at this probe. The relaxation delay was set to 1 s

and 2.65 x 10^4 to 3.6 x 10^5 scans were accumulated for each spectrum. The ^{51}V chemical shifts were referenced to $VOCl_3$, employing V_2O_5 ($\delta = -614$ ppm) as an external standard.[43]

^{51}V ssNMR spectra at 9.4 T were recorded on a Bruker Avance II+ 400 MHz spectrometer operating at a frequency of 105.25 MHz for ^{51}V. Experiments were performed with a 3.2 mm ^{1}H/X/Y triple resonance probe under MAS at a spinning rate of 21 kHz. Spectra were acquired using single-pulse excitation with a pulse length of 0.66 μs. This corresponds to a flip-angle of ca. 30° with respect to a 90° pulse on ^{13}C. The relaxation delay was set to 1 s and 1.8 x 10^5 scans were accumulated for each spectrum. The ^{51}V chemical shifts were referenced to $VOCl_3$, employing V_2O_5 ($\delta = -614$ ppm) as an external standard.[43]

To avoid a structural change of the vanadia-loaded samples by water adsorption, samples were first dehydrated in 12.5% O_2/He for 1 h at 365 °C in the Linkam reactor, cooled down to 25 °C in pure helium and then transferred via an argon flushed glove box into a watertight NMR rotor. The spectra were analyzed by a least-squares fitting analysis using Lorentzian/Gaussian product functions.

2.10. Modulation-Excitation DRIFTS

ME-DRIFT spectroscopy was performed on a Vertex-70 IR spectrometer (Bruker); the modifications made for recording ME-DRIFT spectra have been described elsewhere.[8,35,44] For each experiment, 90 mg of catalyst was used.

We used the rapid scan mode extension of Bruker's spectrometer software OPUS 7.2. Spectra were measured from 850 to 3800 cm^{-1} with a resolution of 0.5 cm^{-1}, an aperture of 8 mm, and a mirror speed of 40 kHz. A Valco Instruments 4/2 valve (Model E2CA, version ED), communicating with the Vertex 70, was used to rapidly switch between different gas feeds, which were controlled *via* digital mass flow controllers (Bronkhorst).

As gases we used C_3H_8 (Westfalen, 3.5), C_3D_8 (Eurisotope, 98% isotopic labeling), O_2 (Westfalen, 5.0), and helium (Westfalen, 5.0). One measurement series consisted of 20 periods, each of which had a duration of 360 s and consisted of 240 spectra. During each period, the gas-phase was switched after 120 spectra and back to the initial gas-phase with the start of the new period. For one spectrum, five

consecutive interferograms were averaged, so that a new spectrum was acquired every 1.54 s.

As background, the catalyst spectrum itself was used, after 60 min of dehydration in 12.5% O_2/helium atmosphere at 365 °C and a 10 min treatment at 320 °C in one of the reaction gases for conventional ME-DRIFTS (12.5% O_2 or 12.5% C_3H_8 in helium) or in reaction gas atmosphere (12.5% C_3H_8/12.5% O_2/75% He) for isotope ME-DRIFTS. The flow was kept constant at 100 mL_n/min during the pretreatment and experiment.

During conventional ME-DRIFTS, a flow of either 12.5% C_3H_8 or 12.5% O_2 in helium was kept constant over the sample, while the other feed gas was pulsed over the sample. In our isotope ME-DRIFTS experiments, the propane-h8-containing reaction atmosphere was switched to a propane-d8-containing reaction atmosphere, while the flow of oxygen through the reaction chamber was constant.

During all ME experiments the temperature was kept at 320 °C. To remove the gas-phase contribution, we subtracted gas-phase phase-sensitive detection (PSD) spectra over KBr (see Figure S1) from each recorded DRIFT spectrum. To exclude the possibility of intensity fluctuations over multiple periods, we checked the intensity profile at three distinct wavenumbers, representative of the background, an adsorbate peak, and a gas-phase peak, but detected no absolute intensity changes over multiple periods that could influence the Fourier transform (see Figure S2). Peak-fitting analysis of ME-DRIFT spectra was performed using Lorentzian functions employing the Levenberg–Marquardt algorithm implemented in OriginLab 2018.

To obtain phase-sensitive spectra, the time-resolved 3D spectral data was converted from the time to the phase domain. For an overview, the resolution of phase spectra was chosen to be 30°, whereas mechanistic insights were obtained using a resolution of 1°. The main operation of PSD is a Fourier transform according to[45]

$$I_{\tilde{v}}(\varphi) = \frac{2}{T} \int_0^T I_{\tilde{v}}(t) \cdot \sin(2\pi f t + \varphi)\, dt$$

where $I(t)$ is the time-dependent intensity at one specified wavenumber ($\tilde{v}$) that is convoluted with the sine function representing the modulation of the external parameter (e.g., the gas-phase concentration), thus forming $I(\varphi)$, the phase-resolved intensity. The frequency of the external modulation is f, whereas 0 and T represent the times at which the considered dataset begins and ends, respectively. To obtain a

complete phase-resolved spectrum, this procedure is repeated for every wavenumber. By varying φ from 0 to 360° with a chosen resolution and repeating the steps above, the complete phase-resolved dataset is created.

To obtain time constants for a particular wavenumber, first the phase angle in the PSD function is determined where $I(t)$ shows the best overlap with the external modulation function. This is done for a set of chosen peak positions. To this end, the phase angle corresponding to the phase spectrum with the largest signal at the particular wavenumber is extracted by automatically comparing the intensities for spectra of all the different phase angles. The following equation is used to translate this phase angle back into a time value within the interval of one period, in order to make it more interpretable:

$$t_{per} = (360 - \varphi_{max})360 \cdot t_{per}$$

The experimental error is 1.54 s, which represents the measurement time of one spectrum. For the temporal analysis of the vanadyl peak, the time constants of the overtones were considered due to their much higher accuracy in comparison to the fundamental vibration (see Figure S3), as discussed previously.[8] Further details of the used software and the full code, which is available free of charge at GitHub, can be found elsewhere.[46]

3. Results and Discussion

In the following, the results for the P25-based samples (VO_x/TiO_2) will be discussed. The results for the SBA-15-based $VO_x/TiO_2/SiO_2$ samples are presented in the Supporting Information (SI) and will be discussed there, establishing a detailed structural model describing the layered ALD system. They will be referenced throughout the manuscript as an addition to the points made in the following.

3.1. Characterization

The P25 samples were first characterized regarding their electronic and geometric structure. Figure 1 shows their UV-Vis spectra, determined band gap energies and XRD patterns. The UV-Vis spectra and XRD patterns of the $VO_x/TiO_2/SiO_2$ samples are given in the SI (see Figure S4) and will be discussed there. Tauc plots were used to determine the band gap energies (see Figures S5 and S6). The wavelengths at which Raman spectroscopy was performed are marked in the UV-Vis spectra because they are highly important for the selective enhancement of Raman intensities, as will be discussed below.
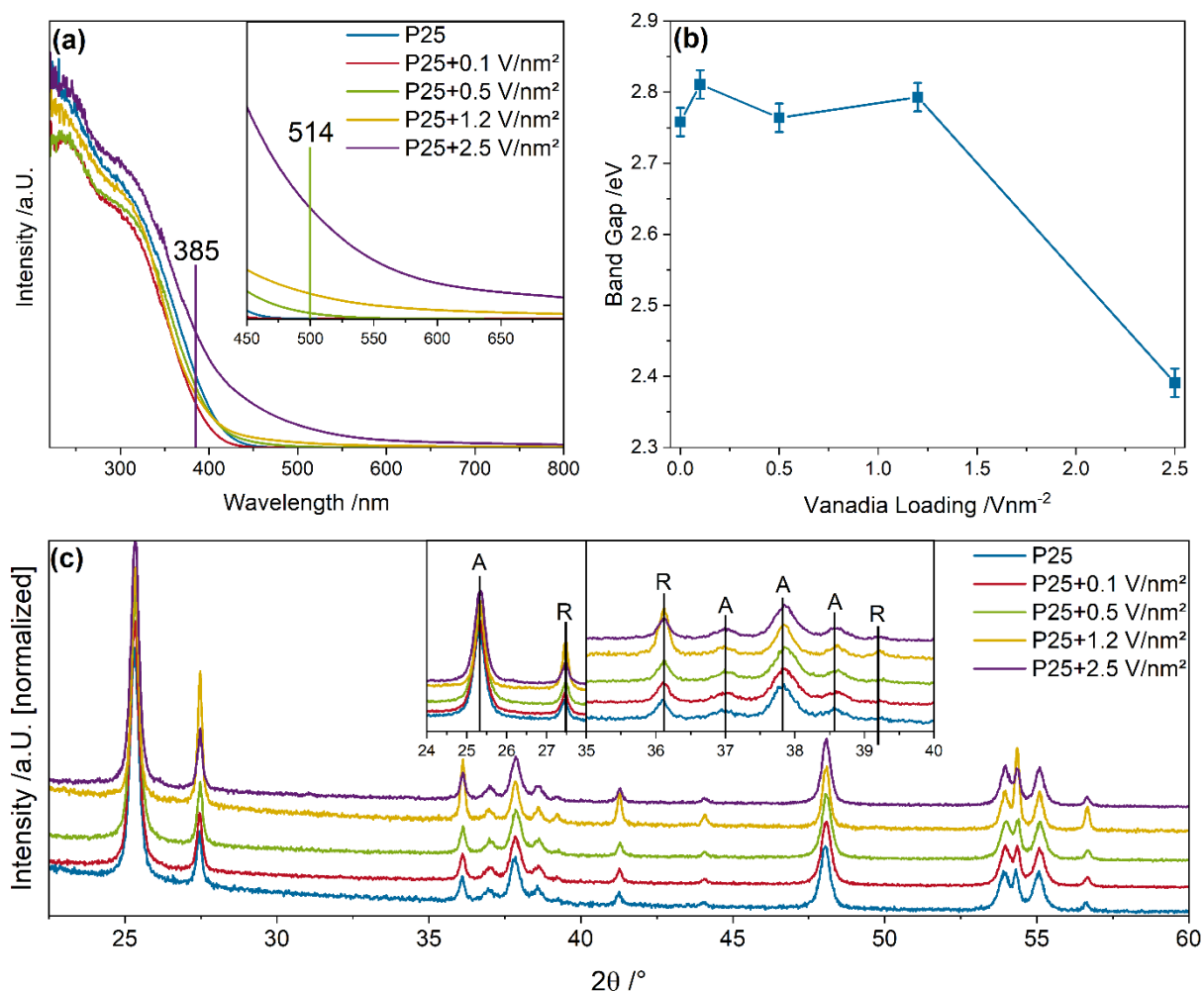
Figure 1: Structural characterization of VO$_x$/TiO$_2$: **(a)** UV-Vis spectra of bare P25 and vanadia-loaded samples. The inset provides an enlarged view of the visible region. The used Raman excitation wavelengths are marked. **(b)** Band gaps of bare P25 and vanadia-loaded samples as determined from Tauc plots. **(c)** XRD patterns of bare P25 and vanadia-loaded samples. In the insets the reflexes assigned to rutile and anatase within 24-28 and 35-40° are marked. The spectra and diffractograms were recorded under pristine conditions after dehydration in 12.5% O$_2$/He for 1 h at 365 °C and subsequent cooling to room temperature.

Figure 1a depicts the UV-Vis spectra of bare and vanadia-loaded P25 samples. The optical properties of titania and its different phases have been studied extensively[47] and the absorption below 400 nm is dominated by the TiO$_2$ absorption of P25, which contains anatase and rutile, and exhibits transitions at 203, 232, and 310 nm, as well as at 168 and 154 nm.[48,49] A contribution from TiO$_2$ in the rutile phase is located at absorption energies lower than those of anatase, red-shifting the observed absorptions.[50] Within the same region, the absorptions from monomeric and dimeric vanadia are expected[31,51] but due to the high titania absorption, their exact contribution is hard to determine. Despite the additional absorption of vanadia below 400 nm, the

overall absorption is lower for vanadia-loaded P25 samples, except for the P25+2.5 V/nm² sample, which may be caused by a perturbation of the TiO_2 conduction band by the V 3d orbitals.[52] This effect might be compensated by the high amount of vanadia loaded onto the P25+2.5 V/nm² sample, leading to a stronger increase in absorption than the decrease caused by the perturbation. Such a behavior is confirmed by the increased absorption of the higher-loaded samples compared to P25+0.1 V/nm². Above 400 nm, the dominance of the titania absorption decreases and higher vanadia nuclearities (oligomers) start to contribute, dominating the absorption at ~450 nm.[31] Here, the P25 sample with 0.1 V/nm² shows no significant absorption, indicating that no oligomerized species are present. The absorption then increases nearly linearly for the P25 samples loaded with 0.5 and 1.2 V/nm², pointing to a small amount of oligomerized species but the overall absorption is still comparably small. For the 2.5 V/nm² sample, the absorption increases much more significantly, indicating that a significant amount of oligomerization of vanadia occurs between 1.2 and 2.5 V/nm², changing the surface chemistry of the sample. The absorption for this sample increases between 275 and 600 nm. As different vanadia nuclearities absorb at different wavelengths[31] and the increase in absorption observed in the UV-Vis spectrum is not the same at all wavelengths, this can lead to differences in nuclearity-dependent resonance enhancements between the two excitation wavelengths used for Raman spectroscopy.

The band gap energies determined from Tauc plots are shown in Figure 1b. The typical band gap energies for titania have values between 2.7 and 3.3 eV, depending on their composition, where anatase is closer to 3.2 eV and rutile closer to 3.0 eV but the presence of oxygen vacancies further decreases the band gap to below 3.0 eV.[53,54] In addition, highly oligomerized vanadia can also red-shift the band gap energy, due to the absorption between 400 and 450 nm.[31] The band gaps of bare P25 and P25 loaded with vanadia up to 1.2 V/nm² reveal, within the margin of error, very similar band gap energies that are only slightly lower than those of bare P25 due to the presence of surface vanadia species and are all in the range between 2.7 and 2.9 eV.[52] This is in good agreement with literature values of defective titania samples.[53,55] When the loading is further increased to 2.5 V/nm², the band gap decreases significantly in concurrence with the sharp increase in absorption above 400 nm. The decrease in the band gap energy can be attributed to the tailing of the absorption caused by the

presence of oligomerized vanadia as well as the charge-transfer transition from d-orbitals of V^{4+} to the conduction band of TiO_2.[56,57]

Figure 1c shows the XRD patterns of the P25-based samples. As P25 is composed of 77% anatase, 16% rutile, and 7% amorphous titania,[58] there are reflexes from the anatase and the rutile phase. The half-width of the reflexes indicates the presence of crystallites with a significant size of >15 nm (determined using the Scherrer equation). The overall shape and line-width does not vary with the vanadia surface density and no additional peaks are present at the highest loadings, indicating only amorphous vanadia or crystallites with a size below the XRD detection limit. The P25+1.2 V/nm² sample shows a slightly higher intensity in the rutile-related reflexes, which might be caused by a not fully inert sample transfer. As the support is a commercial one and the same for all samples, we conclude that this is likely caused by a slightly different pretreatment of the sample. However, this has no effect on the operando/transient spectra shown below, as each of the measurements was performed with a fresh sample.

Figure 2 shows the results of the multi-wavelength Raman spectroscopic characterization of VO_x/TiO_2 with UV (385 nm) and visible (514 nm) laser excitation. The corresponding Raman spectra of $VO_x/TiO_2/SiO_2$ are provided in the SI (see Figure S7) and are discussed there in detail. An exemplary fit of the P25+1.2 V/nm² sample, used to quantify the vanadia-related features from the Vis-Raman spectra, is shown in Figure S8.
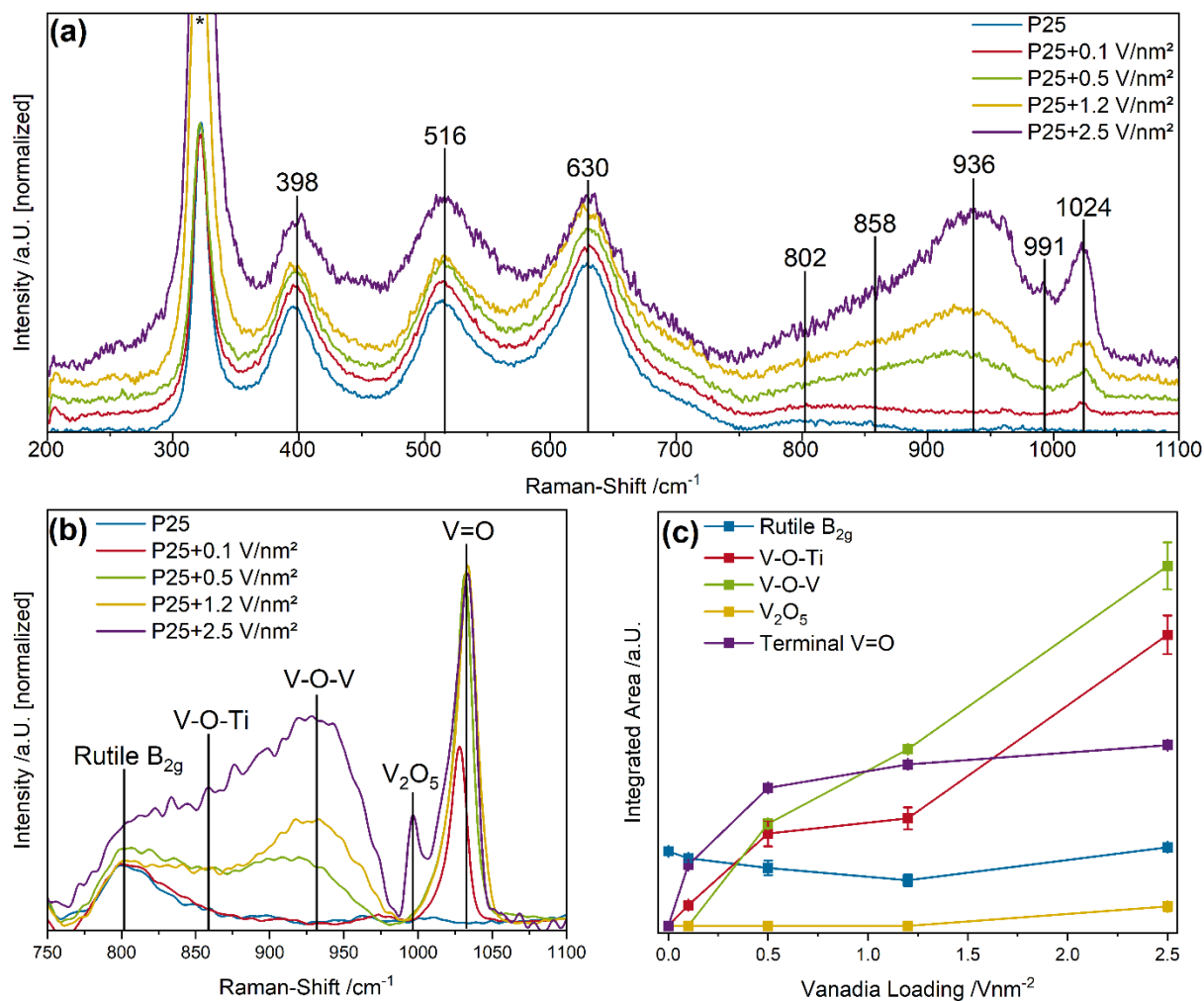
Figure 2: Raman characterization of VO$_x$/TiO$_2$: **(a)** Normalized UV-Raman spectra (385 nm) of bare P25 and vanadia-loaded samples. The signal from the used CaF$_2$ window is marked with an asterisk. **(b)** Normalized Vis-Raman spectra (514 nm) of bare P25 and vanadia-loaded samples used for quantification of vanadia features via deconvolution based on Lorentzian functions **(c)**. All spectra were recorded after dehydration in 12.5% O$_2$/He for 1 h at 365 °C and subsequent cooling to room temperature.

Figure 2a shows the UV-Raman spectra of bare and vanadia-loaded P25 within the phonon region after 1 h of dehydration in 12.5% O$_2$/He at 365 °C and subsequent cooling to room temperature. As the excitation wavelength is located within the region of titania absorption (see Figure 1a), an intensity increase due to resonance enhancement would be expected for titania. Titania features are located at 398, 516, 630, and 802 cm^{-1} and can be assigned to different anatase and rutile phonons. The vanadia-related features at 858, 936, 991, and 1024 cm^{-1} are attributed to interface V-O-Ti, bridging V-O-V, the terminal vanadyl bond of V$_2$O$_5$, and the terminal vanadyl bond of amorphous vanadia, respectively. A feature at 936 cm^{-1} was previously reported to be indicative of V^{4+} species or V-O-Ti bonds. However, the presence of V^{4+} species

19

can be ruled out, due to the significantly smaller Raman scattering cross-section compared to V^{5+} species.[59] Furthermore, V-O-Ti bonds were ruled out since the lowest-loaded sample (P25+0.1 V/nm^2) shows no intensity at 936 cm^{-1} despite the presence of V-O-Ti bonds, as evidenced by the intensity recorded at 858 cm^{-1}, while all higher loadings show significant intensity at 936 cm^{-1}, consistent with the above assignment of this Raman feature to V-O-V bonds exclusively. Table 3 summarizes the Raman assignments for all samples.

Table 3: UV- and Vis-Raman assignments of bare titania and vanadia-loaded samples.

Position /cm^{-1}	Assignment	Reference
398	B_{1g} anatase	60
516	A_{1g} & B_{1g} anatase	60
630	E_g anatase	60
802	B_{2g} rutile	60
858	V-O-Ti	61
936	V-O-V	59
991	V=O of V_2O_5	27
1020-1030	V=O of VO_x	31

Figure 2b depicts the phonon region of the Vis-Raman spectra assigned to vanadia-related features. The excitation wavelength was located within the absorption of oligomerized vanadia to facilitate the quantification of vanadia-related features, avoiding the influence of TiO_2 absorption. The same peaks are observed as with 385 nm excitation but with higher intensity. The peaks were then quantified by using a fit analysis with Lorentzian functions (see Figure S8), yielding the results shown in Figure 2c. The rutile B_{2g} mode overlaps with the vanadia-related features but does not change significantly with the vanadium loading. We therefore conclude that the phase composition of P25 is not affected by the amount of surface vanadia, which is in good agreement with the XRD results.

The 0.1 V/nm^2 sample is characterized by features from terminal V=O bonds of amorphous VO_x and V-O-Ti bonds appear, while no V-O-V related features are detected, indicating that at the lowest loading vanadia is present in its monomeric form, which is consistent with the absorption at ~450 nm being absent for the sample (see Figure 1a). When the surface density is increased, the amount of terminal V=O and V-

O-Ti bonds increases accordingly, while at a loading of 0.5 V/nm² V-O-V bonds can be detected for the first time, indicating that vanadia starts to form surface species with higher nuclearity. When the VO_x surface density is increased to 1.2 V/nm², the V=O and V-O-Ti peaks show a further increase, but the V-O-V intensity increases more significantly, which suggests that cross-linking of vanadia species is an important process at these loadings, whereas the formation of new V-O-Ti bonds is less likely. For the sample with the highest loading, small amounts of V_2O_5 are formed in addition to an increase in all vanadia-related signals, except for the terminal V=O bond of amorphous vanadia, which only increases slightly. The V=O signal of V_2O_5 is not included in the amount of the quantified V=O shown in Figure 2c. For this loading, the V-O-Ti peak shows again a significant increase, since the amorphous 3D particles might add additional linkage to the titania support while new chains are also formed, in line with the significant V-O-V intensity increase due to 3D cross-linking.

Note that the Raman cross-section of vanadyl in V_2O_5 has been estimated to be at least 5 times larger than that of dispersed vanadia, confirming that only small amounts of V_2O_5 are formed.[62,63] Thus, the very small amount of V_2O_5 present on the surface is not expected to have a significant influence on the catalyst`s behavior. As the monolayer coverage of oligomeric VO_x on titania is normally described to be much higher than 2.5 V/nm² (7.5-7.9 V/nm²),[64–66] the formation of V_2O_5, that is, the oligomerization of vanadia is likely to be caused by the large number of defects in P25, as determined from the measured band gap energies (see Figure 1b). Even though the SBA15-T+1.2 V/nm² sample shows a much lower VO_x defect density, it still contains V_2O_5 on the surface. This is not necessarily a contradiction since the titania phase of the ALD-synthesized sample is almost fully amorphous and the SBA-15 support possesses pores coated by titania, in which vanadia might be crowded, inducing the formation of V_2O_5, even at lower loadings, and despite the lower defect density. The presence of small amounts of V_2O_5 would also explain the increased absorption intensity above 400 nm in the UV-Vis spectra (see Figure 1a). Due to the presence of V_2O_5, amorphous 3D particles are also likely to be present on the surface, which contain vanadium atoms linked by V-O-V, contributing to the steep increase of V-O-V in comparison to V-O-Ti and V=O.

Additionally, the resonance enhancement of oligomers leads to a stronger increase in V-O-V intensity as well, unlike V=O, which is also present in monomers, which are only resonantly enhanced in the UV range. The discrepancy in the loading-

dependent V=O intensities between the UV- and Vis-Raman spectra is well explained by the different resonance enhancements of the different nuclearities and the different absorption increases in the UV-Vis spectra of P25+2.5 V/nm², as discussed above (see Figure 1a). This leads to a much larger increase in the V=O signal for this sample at the 385 nm excitation wavelength than for the 514 nm excitation wavelength, which is further underlined when the loading-dependent V=O intensity is compared for both excitation wavelengths (see Figure S9). The presence of resonance enhancements is supported by the small intensities of the V=O and V-O-V overtones observable for the P25+2.5 V/nm² sample in the UV-Raman spectra, while they are barely visible for lower loadings due to the overlap with the overtone of the rutile E_{2g} mode (not separately shown) and their low intensities. Furthermore, the amount of rutile is very important for the degree of oligomerization of vanadia on titania, as the presence of some rutile in the anatase phase increases the mobility of the vanadia species.[67] All in all, vanadia starts to form 3D particles much more readily on P25 than would be expected from the typical value of the monolayer coverage. Translating this behavior to the P25 samples with lower vanadia loadings may result in a higher degree of V-O-V bonds than would be typically expected.

For the SBA-15 based $VO_x/TiO_2/SiO_2$ sample, XPS measurements (see Tables S1 and S2 and Figures S10 and S11) and nitrogen physisorption analyzed by the BET method are shown in the SI and combined with the UV-Vis, XRD and multi-wavelength Raman data to establish a structural model of the layered ALD system, which will be used as a reference in the context of the mechanistic interpretation.

3.2. Catalytic Activity and Operando Spectroscopy

Before the operando spectroscopic measurements were made, the catalytic activity of the catalyst was measured. Figures 3a and b present temperature-dependent conversions and selectivities for bare and vanadia-loaded P25 samples, while Figures 3c and d present the loading dependence of the conversions and selectivities at 320 °C. Temperature-dependent conversions and selectivities of the $VO_x/TiO_2/SiO_2$ sample are given in the SI (see Figure S13).
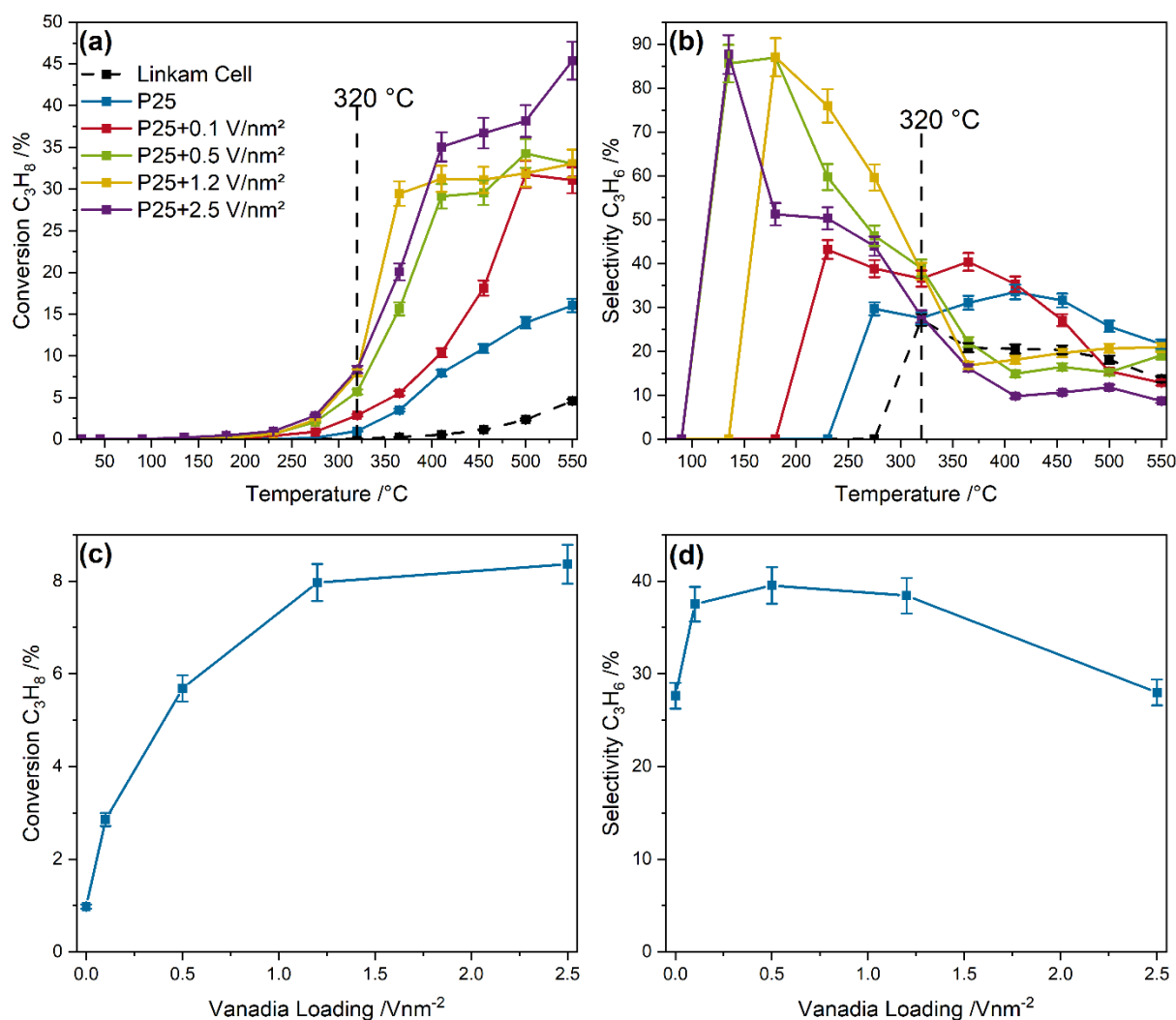
Figure 3: Reactivity behavior of VO$_x$/TiO$_2$ in propane ODH: Temperature-dependent **(a)** conversions and **(b)** selectivities of bare P25 and vanadia-loaded samples and the empty reaction chamber. The temperature at which operando spectroscopy was performed is marked. Loading-dependent **(c)** conversions and **(d)** selectivities of bare P25 and vanadia-loaded samples at 320 °C.

Figure 3a shows the temperature-dependent propane conversion over bare and vanadia-loaded P25 samples, which is smallest for bare P25 but increases with the vanadium loading, in particular from 0.1 V/nm² to 0.5 V/nm². For comparison, the behavior of the empty Linkam reactor is shown, which shows conversions that are significantly smaller than those of the catalyst samples. At a temperature of 320 °C, conversions of <0.05 % are measured, which are within the margin of error. Therefore, we exclude any contributions of homogeneous gas-phase reactions or the reactor at the temperature chosen for the operando spectroscopy. Figure 3b depicts the corresponding selectivities towards propylene. For bare P25, the selectivity stays almost constant at around 30% for all temperatures, indicating that the oxygen mobility

in titania has no significant influence on the observed selectivities. The vanadia-loaded samples have a very high selectivity of 80%-90% at low temperatures, where the conversions are <0.1%, but show a decline to 40%-50% as the conversions start to increase to a significant level at ≥275 °C. Up to 400 °C the selectivities of the vanadia-loaded P25 samples are higher than for bare P25 despite the higher conversions, indicating that the vanadia loading significantly changes the surface chemistry of the catalyst which leads to a different reaction mechanism. A temperature of 320 °C was chosen for the spectroscopic investigation, as the vanadia-loaded samples and even the bare support show significant conversions and selectivities that can be detected reproducibly. The loading-dependent conversions and selectivities for bare and vanadia-loaded P25 samples at 320 °C are summarized in Figures 3c and d. The conversions first increase significantly with increasing vanadium loading but then level off, especially for the increase from 1.2 to 2.5 V/nm², which is consistent with previous studies reporting no dependence of the conversion on the surface density above 2.5 V/nm².[3] As shown in Figure 3d, the selectivity for bare P25 is about 30%, increases to 38% for a loading of 0.1 V/nm², then stays constant within the margin of error and finally starts to decrease back to 30% at a loading of 2.5 V/nm². Besides propylene, the only products detected were CO and CO_2, and carbon on the catalyst surface. The selectivity behavior is mostly explained by the different conversions (see also discussion below), but for the highest loading, the higher degree of oligomerization (i.e. the large number of V-O-V bonds) and the presence of V_2O_5 might explain the decline in selectivity while the conversion stays constant.

There are a number of kinetic studies on propane ODH over VO_x/TiO_2 catalysts available in the literature,[5,6,23–29,68] covering a variety of titania supports, temperatures and vanadia loadings. Our activity data is similar to results reported for a fixed bed reactor operated closest to our conditions, indicating the comparability of the Linkam reactor to a fixed bed reactor,[5,23] as discussed previously.[7] Especially the loading-dependent conversions reported in this study show a very similar course when compared to literature data acquired at the same temperature and for the same range of vanadium surface densities,[23] while the corresponding selectivities are in line with reported fixed bed reactor results.[5]

Figures 4a and b show the UV-Raman spectra of bare P25 and P25+1.2 V/nm² samples during oxidizing and reactive conditions as well as Vis-Raman data of the vanadyl region in the inset. The UV- and Vis-Raman spectra for the other P25 and

ALD-synthesized samples are given in the SI (see Figures S14 and S15). The observed intensity changes were quantified by a peak-fit analysis using Lorentzian functions (see Figure 4c). An exemplary fit of the vanadyl region in the UV-Raman spectrum of the P25+1.2 V/nm² sample is given in the SI (see Figure S16).
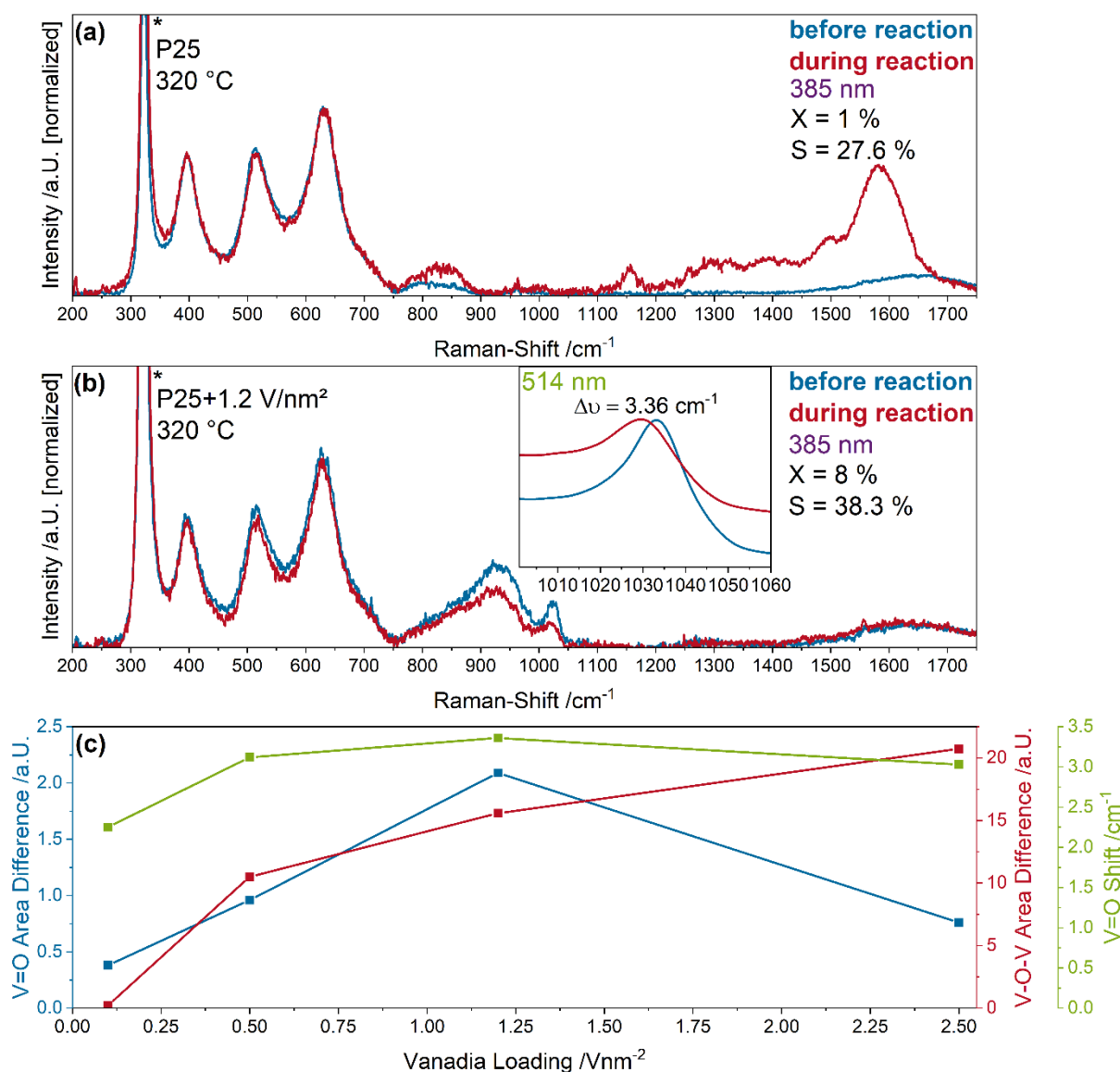
Figure 4: Normalized UV-Raman (385 nm excitation) spectra of **(a)** bare P25 and **(b)** P25+1.2 V/nm² recorded at 320 °C under oxidizing (blue; 12.5% O_2/He) and reactive (red; 12.5% O_2/12.5% C_3H_8/He) conditions, characterized by the given conversions and selectivities. The peak originating from the used CaF_2 window is marked with an asterisk. The inset shows the Vis-Raman spectrum (514 nm) of the vanadyl peak. **(c)** Observed intensity changes of the vanadia-loaded samples. The operando UV-Raman spectra for the other samples as well as an exemplary fit are given in the SI (see Figures S14-S16).

In Figure 4a, UV-Raman spectra of bare P25 are shown. Exposure to reaction conditions leads to an increase in the intensity of the rutile B_{2g} peak at 820 cm^{-1}. In the literature, this peak is normally described as a low intensity Raman feature, which highlights the selective enhancement of TiO_2.[60] The absorption maximum of rutile is also closer to the excitation wavelength than that of anatase, leading to more absorption in the near visible UV region for rutile than for anatase, which is in good agreement with the observed enhancements in the Raman spectra. Additionally, multiple peaks in the region between 1100 and 1750 cm^{-1} appear, which can be assigned to different amorphous carbon species on the surface.[69,70] The sharp peak at 1150 cm^{-1} is not compatible with this assignment and has been attributed to carbon in hexagonal diamond configuration.[71] This indicates that over bare P25 a significant part of the converted propane is deposited as carbon on the surface, which however cannot be caused by oxygen depletion, as the samples with the largest carbon deposits (P25 and P25+0.1 V/nm²) use the least oxygen, showing oxygen consumptions of 4 and 11%, respectively (see Figure S17). As can be seen by the change of the rutile band at 820 cm^{-1} upon exposure to reaction conditions, a TiO_2 phase-transition occurs, partially transforming anatase to rutile as nanocrystals, as the change is not detectable by XRD (see operando XRD results in Figure S18). This phase transition might be linked to oxygen vacancy formation, as oxygen vacancies are more easily formed at the boundary between the anatase and rutile phases and can facilitate a phase transition.[53] The amount of transformed titania is probably small due to the low conversion of bare titania, and is expected to lead to only a small amount of oxygen vacancies because titania shows a lower oxygen mobility than other supports such as CeO_2.[72,73]

When vanadia is introduced, the observed changes in the catalysts` behavior differ significantly, as no more changes of the carbon and rutile features are detected in the Raman spectra (see Figure 4b). Instead, there are apparent intensity changes of the vanadia features related to V-O-V and V=O. Additionally, a significant red-shift of the vanadyl position can be observed in the Vis-Raman spectra (see inset). This behavior is consistent with a decrease in V-O-V intensity, as the breaking of V-O-V bonds reduces the average nuclearity of vanadia and hence the degree of dipole-dipole coupling between the vanadyl groups, resulting in a red-shift of the vanadyl position.[32] This red-shift occurs concurrently to a significant intensity decrease of the V=O peak intensity in both UV- and Vis-Raman spectra, as well as a significant

decrease in V-O-V intensity in the UV-Raman spectra. The same intensity changes are observed for the 0.5 V/nm² and the 2.5 V/nm² samples (see Figure S14), whereas the 0.1 V/nm² sample is characterized by a mixture of the bare titania and vanadia-related dynamics. That is, the rutile band increases and the carbon features appear, but to a lesser degree than for bare P25, and the vanadyl feature shows a red-shift and an intensity decrease. For this sample, no V-O-V dynamics are observed, consistent with the presence of monomeric vanadia species, as discussed above.

The intensity changes of all vanadia-loaded P25 samples (V=O shift, V=O and V-O-V area differences) upon exposure to reaction conditions is summarized in Figure 4c. Starting with the V-O-V dynamics, the observed trend correlates well with the determined conversions (see Figure 3c), whereas the vanadyl area change and position follow the trend only up to a surface density of 1.2 V/nm². For the P25+2.5 V/nm² sample, the V=O area change and V=O position decrease in comparison to the P25+1.2 V/nm² sample, and only the V-O-V area change increases significantly, while the conversion stays almost unchanged between 1.2 and 2.5 V/nm². This behavior suggests that both V=O and V-O-V oxygen atoms can support propane ODH but, at higher loadings, the high amount of V-O-V oxygen becomes the dominant oxygen site where, based on UV-Vis characterization (see Figure 1), more oligomeric species are present. As the conversion stays constant but the selectivity decreases between these samples, V-O-V bonds of oligomeric vanadia appear to be less selective than vanadyl oxygen. This trend becomes even more apparent when the SBA-15-based sample is considered, which is dominated by V=O dynamics (with very little V-O-V dynamics) and has a higher selectivity (see Figure S15 and discussion). This indicates that the reactivity behavior depends on the detailed vanadia site, specified by the type of oxygen atom as well as its nuclearity.

For VO_x/CeO_2, it was possible to determine the distribution of different nuclearities on the surface from the vanadyl signal from either Raman or IR spectroscopy,[7,32] but for other catalyst systems, such a detailed vanadyl fine structure has not been detected. To identify the significant vanadia sites on the P25-based catalysts, we applied a combination of Raman spectroscopy and ^{51}V ssNMR spectroscopy. As V^{4+} and V^{3+} species have very short relaxation times due to their paramagnetic character, the ssNMR spectra show only signals attributed to V^{5+} species, enabling a direct comparison with Raman results.[42,59] Note that V^{5+} species located close to paramagnetic species such as reduced vanadia or titania may not be

observed in the spectra due to paramagnetic bleaching. Since ssNMR spectra of the P25+1.2 V/nm² sample obtained at different field strengths reveal a significant contribution from second-order quadrupolar interactions (see Figure S19), the identification of various vanadia species via ssNMR line-shape analysis of the sideband pattern to extract the quadrupolar and the chemical shift anisotropy parameters is not feasible. The same is valid for the quantification of the vanadia species. Thus, a qualitative analysis of the isotropic signals obtained in the spectrum of the P25+1.2 V/nm² sample measured at 14.1 T and 21 kHz spinning was performed by using a peak-fit analysis with three Lorentzian/Gaussian product functions (see Figure 5a). The results can be compared to those obtained for the vanadyl region from UV-Raman spectra (see Figure 5b). The NMR spectra of P25+1.2 V/nm² are characterized by three signals located at ~-508, ~-530, and ~-564 ppm, which have previously been attributed to two monomeric sites (ordered and distorted) and dimeric sites, that are doubly bridged by V-O-V, respectively.[67,74,75] Interestingly, the isotropic signal shows no contributions from higher oligomerized species that would all be present above -600 ppm. This might be due to the unique interaction of P25 with vanadia or to the complete absence of water, which would facilitate the oligomerization of vanadia if present.[76–78]

Since for the P25+1.2 V/nm² sample only signals from monomeric and dimeric species are detected, it stands to reason that samples with lower loadings also contain only monomeric and dimeric species. For the P25+2.5 V/nm² sample, the significantly increased absorption at ~450 nm (see Figure 1) points to the presence of vanadia species with a higher degree of oligomerization, as discussed above. Thus, the vanadyl peaks in the Raman spectra of the P25-based samples were fitted by using one component for the P25+0.1 V/nm² sample (only monomers; see Figure S14), two components for the P25+0.5 V/nm² and P25+1.2 V/nm² samples (monomers, dimers), and three components for the P25+2.5 V/nm² sample (monomers, dimers, oligomers), i.e., by including species with a higher degree of oligomerization. The fact that the vanadyl fine structure in the Raman spectra comprises only two contributions is fully consistent with the exclusive presence of monomeric and dimeric species at loadings up to 1.2 V/nm². This approach is also in very good agreement with the shapes of the vanadyl peaks. To obtain accurate peak areas, the position of the monomeric species was determined from the spectrum of the 0.1 V/nm² sample and fixed when fitting the spectra of the other samples. The results of the quantification of monomeric and

dimeric species are shown in Figure 5c, together with the conversions of each sample and the percentage of dimeric species to the overall amount of vanadia loaded onto the sample.

For validation, the same approach for quantification of vanadia nuclearities by combining NMR and Raman spectroscopy was applied to a reference VO_x/CeO_2 system, as in this case the vanadia nuclearity distribution is well known due to the pronounced vanadyl fine structure in the Raman spectra of VO_x/CeO_2 systems, extending from monomeric to oligomeric species.[8,32] This analysis confirms the above assignments and underlines that our NMR method is able to detect oligomeric vanadia structures and to rule out any external effects that would cover the oligomeric species in the NMR spectrum of P25+1.2 V/nm². The results together with their assignments are given in the SI (see Figures S20 and S21 and Table S4).
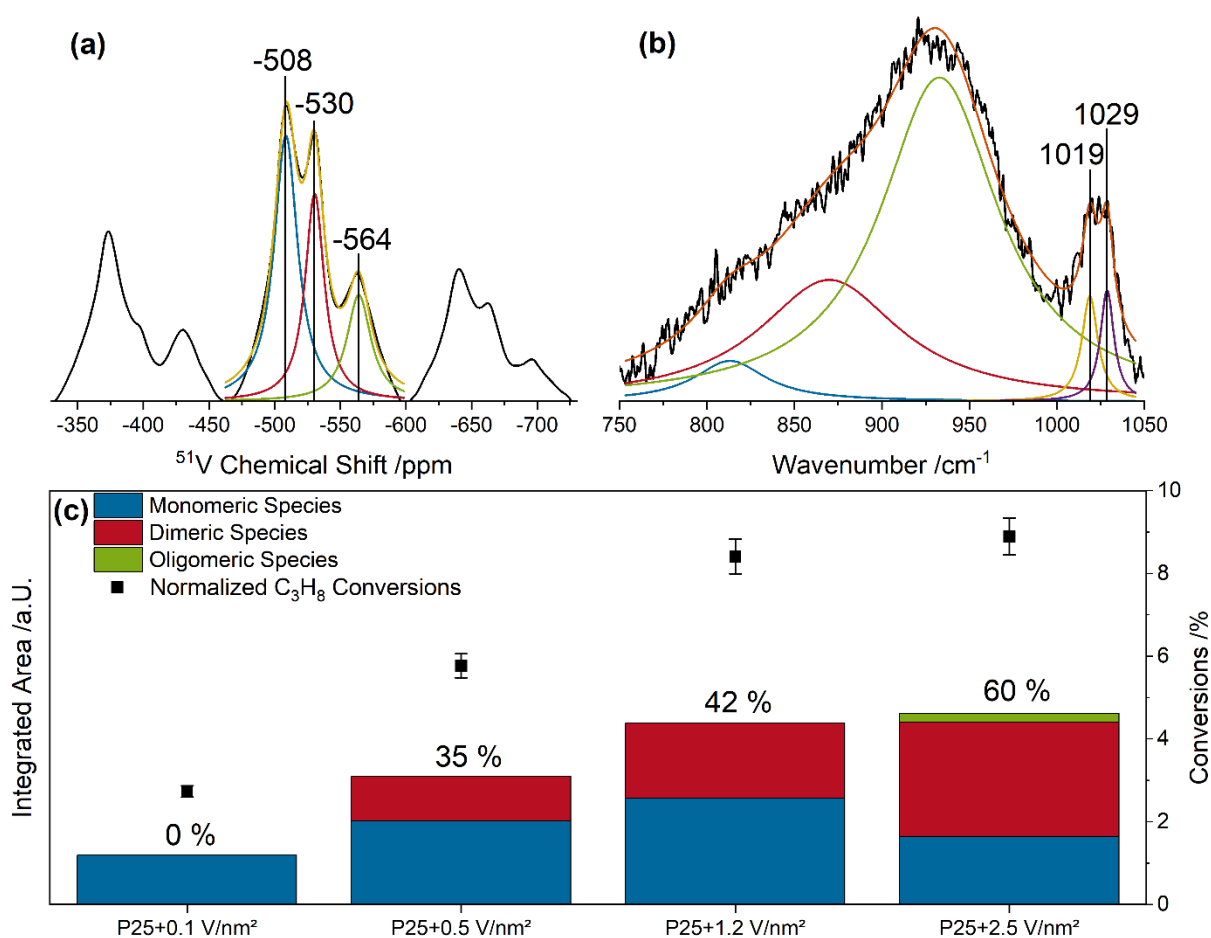

Figure 5: (a) ^{51}V ssNMR spectrum of P25+1.2 V/nm² measured at 14.1 T and 21 kHz rotational frequency referenced to $VOCl_3$ with V_2O_5 as the external standard. The isotropic signal (determined by measurements at two MAS rates, see Figure S19) was fitted using three Lorentzian/Gaussian product

functions. **(b)** UV-Raman (385 nm excitation) spectrum of the vanadia region of P25+1.2 V/nm² together with an exemplary fit, using five Lorentzian functions. **(c)** Quantified areas of the monomeric, dimeric, and oligomeric components of the vanadyl peak in the UV-Raman spectra. The relative amount of dimeric species in relation to the overall amount of vanadia species is given and compared to the propane conversions.

The quantification of the vanadia species from the Raman spectra as outlined above reveals that for the 0.1 V/nm² sample there are only monomers and that the relative amount of dimeric species increases with every loading step. The increase is especially relevant from 0.1 to 0.5 V/nm², where the increase in the conversion is also most significant, as well as from 1.2 to 2.5 V/nm², where there is only a small change in conversion. As discussed in the context of the operando UV-Raman spectra (see Figure 4c), the latter behavior is a result of the shift in composition of surface vanadia species towards dimers, leading to an increased activity due to V-O-V bonds and a decreased activity of the vanadyl oxygen, while simultaneously the selectivity decreases. This significant increase in dimeric species from P25+1.2 V/nm² to P25+2.5 V/nm², as well as the small amount of species with a higher degree of oligomerization (based on the vanadyl deconvolution), is in good agreement with the results from UV-Vis spectra (see Figure 1). The above findings lead to the conclusion that the V=O oxygen is an important site for the selective oxidation of propane. As the introduction of vanadia monomers already triples the catalyst activity compared to bare titania and the increase between bare titania is larger than that from 0.1 to 0.5 V/nm² despite the fact that only 1/5 of vanadium is present, it stands to reason that monomeric species are highly active. In comparison, doubly bridged V-O-V bonds appear to be less preferential to supply the oxygen atoms facilitating propane oxidation up to a loading of 1.2 V/nm². However, the activity shifts at least in part from monomers to dimers, as the participation of V-O-V is clearly evidenced. Thus the V-O-V site plays an important role for the further increase in reactivity, together with the monomers, which contribute to the V=O dynamics. When the loading is further increased to 2.5 V/nm², a significant amount of oligomerized species will be present on the surface (see Figure 1), which are linearly bridged with V-O-V,[75] which becomes the preferential site that is more active but less selective than the previously preferential V=O bond of monomers and dimers due to its better reducibility. As shown in Figure 5c, the conversion scales with the overall amount of vanadia present due to oxidation at both V=O and V-O-V sites.

It does, however, not increase linearly with the vanadium loading, as, at the highest loading, more linear V-O-V sites are formed that replace V=O bonds as the active site. This is further emphasized by the significant decrease of V=O dynamics between 1.2 and 2.5 V/nm² in UV-Raman spectra (see Figure 4c) but still increased V-O-V dynamics concurrently to the appearance of oligomerized vanadia. These also show a lower selectivity, which is in very good agreement with the quantification of the vanadyl peak in Figure 5c. Summarizing, the combination of ^{51}V ssNMR and UV-Raman spectroscopy can lead to an advanced identification and even quantification of the nuclearity- and loading-dependent active vanadia sites in VO_x/TiO_2 catalysts.

To further understand the catalysts´ mode of operation and, in particular, the role of reduced vanadia, which cannot be probed by NMR or Raman spectroscopy, UV-Vis spectroscopy was employed. Figures 6a and b show UV-Vis spectra of bare P25 and P25+1.2 V/nm² under oxidizing (12.5 % O_2/He) and reactive (12.5% O_2/12.5% C_3H_8/He) conditions at 320 °C, while Figure 6c summarizes the structural dynamics of the vanadia-loaded samples. Quantification was performed by fitting the entire UV-Vis spectrum, using Gaussian functions located at the positions of titania[48,49] and vanadia[79] transitions reported in the literature. The operando UV-Vis spectra for the remaining P25 and ALD-synthesized samples are given in the SI (see Figures S22 and S23) and an exemplary fit used for the quantification of UV-Vis spectra is shown in Figure S24.
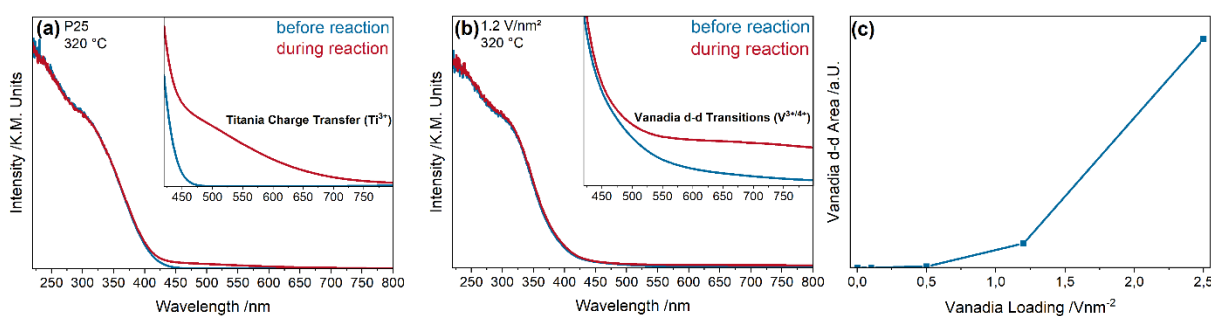
Figure 6: UV-Vis spectra of **(a)** P25 and **(b)** P25+1.2 V/nm² measured under oxidizing (12.5% O_2/He) and reactive (12.5% O_2/12.5% C_3H_8/He) conditions at 320 °C. The insets show enlarged views of the visible region. **(c)** Quantification of the loading-dependent spectral changes.

Starting with the UV-Vis spectra of bare P25, switching from oxidizing to reactive conditions leads to the appearance of a new absorption band at 520 nm that gradually decreases in intensity until its disappearance at 750 nm (see Figure 6a). The detected band can be attributed to a charge transfer transition due to titania reduced from Ti^{4+}

to Ti^{3+} caused by oxygen vacancy formation.[80,81] The band gap shows a slight red-shift, as determined by Tauc plots, which is also caused by defect creation, that is, Ti-OH and oxygen vacancies create new states in the band gap, close to the conduction band, resulting in a decrease of the band gap energy.[55] Both of these effects are rather small and, as the conversions of bare titania samples are small, appear to be caused by propane ODH. This leads to the following mechanistic picture of propane ODH over bare titania samples: propane first interacts with the catalyst, whereby lattice oxygen is then used to oxidize propane, leading to the formation of oxygen vacancies (see Figure 6a) on the interface between anatase and rutile where the defects are favorably formed besides additional rutile (see Figure 4a). In comparison to other oxide supports, titania is difficult to reduce, that is, high temperatures are needed to mobilize lattice oxygen.[72,73] Due to the high temperatures required, propane is often overoxidized or converted to carbon on the catalyst surface once the oxygen becomes mobile, as is apparent from the carbon deposits detected by UV-Raman spectroscopy (see Figure 4a).

For comparison, the UV-Vis spectra of the vanadia-loaded samples do not show a band gap energy shift or a Ti^{3+} charge transfer signal, except for the P25+0.1 V/nm² sample, but a significant intensity caused by vanadium d-d transitions, due to the reduction of vanadium from 5+ to 3+/4+ (see Figure 6b).[78] The spectra of the P25+0.1 V/nm² sample resemble those of bare titania but to a lesser degree, as they already contain features of the vanadia-loaded samples. Figure 6c summarizes the extent of reduction of the P25-based samples, as measured via the d-d transitions, which shows a strong increase with increasing loading. For the P25+0.1 V/nm² sample, the integrated intensity of the d-d transitions is small, which at first sight disagrees with the more pronounced changes seen in the UV-Raman spectra (see Figure 4c), but may be explained by resonance enhancement of the V=O peak caused by the use of UV excitation. In fact, at such low loadings the sample is characterized by the presence of monomeric vanadia species, which experience a resonance enhancement at 350-400 nm,[31] resulting in an increase of the Raman signal not present in the UV-Vis spectra. Likewise, the P25+1.2 V/nm² sample is subject to an enhancement in the UV-Raman spectra due to similar surface vanadia species (see Figure 5), which are now present in larger amounts, and with the addition of dimers, which are more easily reduced, this leads to an increased signal of d-d transitions in UV-Vis spectroscopy. Overall, the

results from UV-Vis spectroscopy are in good agreement with the Raman and NMR results, supporting the proposed behavior of the VO_x/TiO_2 catalysts.

Using static operando experiments, a provisional reaction mechanism can be deduced, which provides answers to three of the four key questions outlined in the introduction, i.e., the definition of the vanadia active site, its nuclearity dependence, and the role of titania in controlling the vanadia structure, including the degree of oligomerization, via its phase composition.[67] The oxygen transfer paths had been followed and can explain most of the activity behavior of the VO_x/TiO_2 systems, but so far there had been no information on the role of the hydrogen dynamics that were previously established to be of significance for propane ODH.[8] Additionally, the structural dynamics on VO_x/TiO_2 samples shown here resembles that of VO_x on an inactive support like SiO_2, as titania does not seem to participate in the reaction itself. To further understand the role of titania in the hydrogen transfers, transient IR spectroscopy was applied due to its potential to provide crucial mechanistic information for alkane ODH reactions.[8]

3.3. Modulation-Excitation-DRIFTS

Figure 7a depicts the PSD spectra of P25-based samples at a phase-angle of 360° during pulsed oxygen and constant propane flow at 320 °C. This specific flow scheme has previously been shown to provide more mechanistic information than a constant oxygen and pulsed propane flow mode.[8] Figure 7b summarizes the loading-dependent quantification of the transient Ti-OH species detected during ME-DRIFTS. Static DRIFTS results (as a reference for the transient results), P25 and P25+1.2 V/nm² PSD spectra with a 30° phase resolution, as well as PSD spectra of all samples at 360° in constant oxygen and pulsed propane flow as well as pulsed oxygen and constant propane flow, are shown in the SI (see Figures S25-S29). For the quantification of the Ti-OH peaks, water rotational bands were removed from the spectrum, and exemplary data processing spectra are shown in Figure S30.
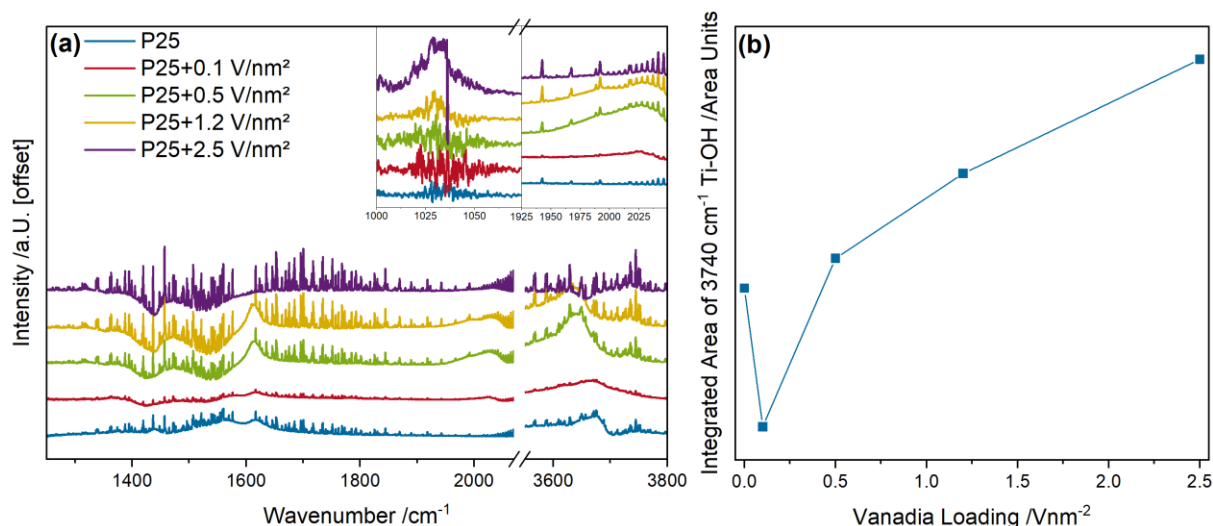
Figure 7: (a) PSD spectra of bare P25 and vanadia-loaded samples in a pulsed oxygen and constant propane flow at 320 °C at a phase-angle of 360°. The insets give an enlarged view of the fundamental and overtone of the vanadyl vibration. The transient Ti-OH species at 3740 cm^{-1} was first corrected for water rotational bands and then quantified **(b)**.

The PSD spectra of P25-based samples in Figure 7a reveal multiple peaks that are not visible in static operando DRIFTS. In the carbonate region, three peaks are most prominent, located at 1438, 1562, and 1618 cm^{-1} and at ~1370, 1480, and 1610 cm^{-1} for bare P25 and vanadia-loaded samples, respectively. These peaks can be assigned to various species of formates and carbonates as well as the propylene C=C double bond.[82,83] For the vanadia-loaded samples, additional peaks appear within 1010-1040 and 1990-2040 cm^{-1}, which can be assigned to the vanadyl fundamental and overtone vibrations.[84] In the Ti-OH region, multiple OH groups can be detected at ~3610, 3640, and 3740 cm^{-1}. These can be attributed to V-OH, isolated Ti-OH on rutile and isolated Ti-OH on anatase, respectively.[84–87] The peaks in the carbonate region, the vanadyl peaks and the Ti-OH groups at 3610 and 3640 cm^{-1} already show dynamics in the static operando DRIFT spectra. All these regions improve significantly in their spectral quality due to the removal of the background, noise and spectator species. Only the Ti-OH peak at 3740 cm^{-1} is not present in static operando DRIFT spectra, but in the PSD spectra of all samples, with varying intensity. It is assigned to a singly-bound Ti-OH group on anatase, which is the dominant phase in P25. Figure 7b shows the integrated areas after removal of the water rotational bands. P25 has a higher amount of transient Ti-OH species than P25+0.1 V/nm², but at higher loadings, starting at 0.5 V/nm², the amount of anatase Ti-OH species correlates very well with

the observed conversions. This indicates that the titania support not only influences the degree of oligomerization of the vanadia species but also participates in the reaction by abstracting hydrogen from propane to the catalyst surface during a quick hydrogen transfer to a more stable species. Thus, the reaction is facilitated by surface oxygen, as has been observed previously for other vanadia-based catalysts.[8] The higher amount of Ti-OH in P25 might be caused by the absence of vanadia, and the consequently sharp slow-down of the reaction rate if no readily reducible oxygen from vanadia is present. Therefore, the otherwise metastable Ti-OH species becomes more prominent, due to a lack of transfer targets that would facilitate a further reaction. When the loading is increased to 0.1 V/nm², the amount of Ti-OH species decreases, as they can be transferred to vanadia. The overall amount for this sample is smaller than for the other samples, due to the lack of V-O-V and V=O species at such low loadings, which would drive the conversion. At higher loadings, the amount of Ti-OH species correlates very well with the conversion, indicating that the initial C-H bond breaking is the rate-determining step that can be catalyzed by the titania surface. As the Ti-OH species was determined to be transient, it is regenerated very fast by the transfer to vanadia. This provides an answer to the fourth question on the role of titania during propane ODH, by demonstrating its direct participation in the rate-determining step, leading to a further increase in the reaction rate in comparison to for example, SiO_2, in addition to the control of the degree of vanadia oligomerization via the phase-composition. This behavior of titania is in agreement with recent studies, which proposed titania to be redox inactive during ethanol ODH.[18] An alternative explanation for the observed behavior may be the dissociation of produced water, which would also correlate with the conversion. However, this is not supported by the higher amount of anatase Ti-OH on bare P25 and P25+0.1 V/nm² where the conversion is lower. Therefore, the observed intensity trend of this peak is in agreement with initial C-H abstraction but not with the dissociation of water after product formation, as a strict correlation of the Ti-OH intensity with the conversion for all samples would be expected.

To investigate the detected transient adsorbates in more detail, the time evolution of the adsorbates was determined by in-phase angle analysis to obtain the time constants for each sample. Exemplary results for the P25+1.2 V/nm² sample are shown in Figure 8 and the values of the time constants are summarized in Table 4. A detailed explanation of the in-phase angle analysis can be found in the experimental

section and in the literature.[8,35] The time constants for the remaining P25-based samples are given in the SI (see Table S5), while time constants were not determined for the SBA-15 based samples, as they only showed significant structural changes in the transient Ti-OH species at 3740 cm^{-1} and no other signals (more details in the SI, Figure S29). As the measurement time of one IR spectrum was 1.54 s, this value was taken as the experimental error of all time constants, as multiple subsequent measurements of the same sample lead to a smaller divergence. For the vanadyl peak, the overtone region was used to determine the time constants due to its better accuracy (compare experimental section and Figure S3).
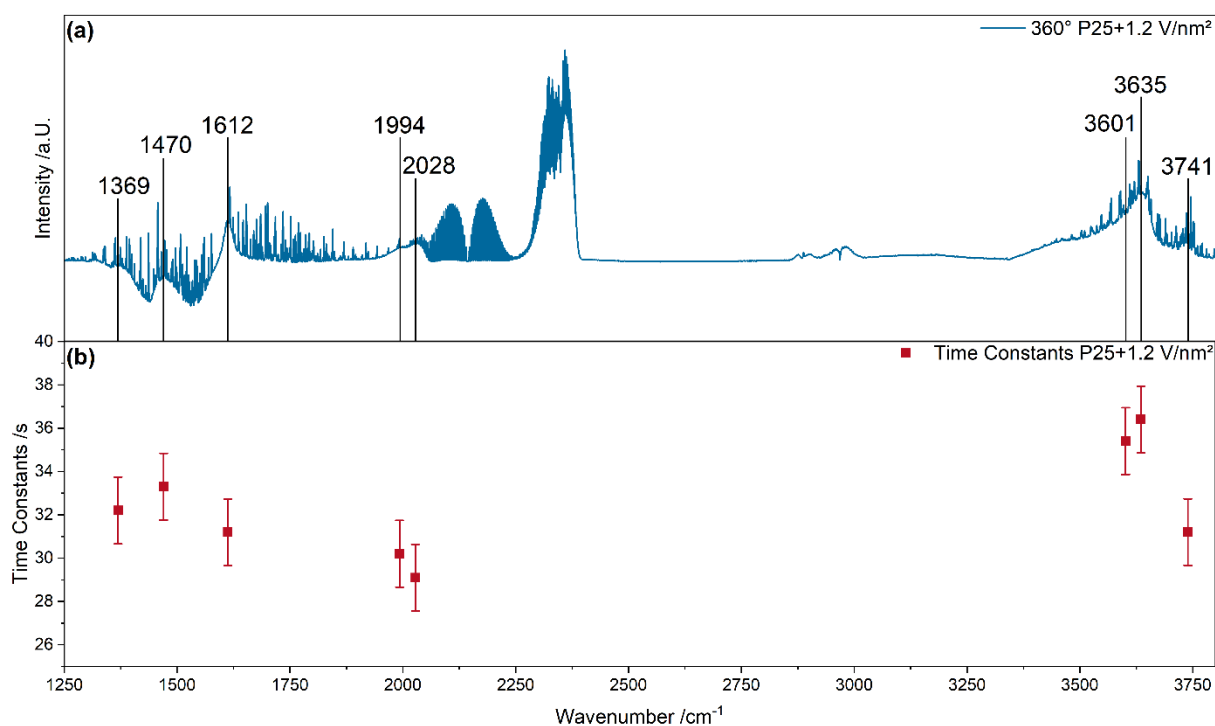
Figure 8: (a) PSD spectrum of the P25+1.2 V/nm² sample at a phase-angle of 360 °C measured at 320 °C in a constant oxygen and pulsed propane flow. The features analyzed by in-phase angle analysis are marked and the respective time constants are given in the lower plot **(b)**, together with the experimental uncertainty.

Table 4: Time constants of the P25+1.2 V/nm² sample determined from in-phase angle analysis of PSD data with a 1° phase angle resolution. The time constants of the other samples are given in the SI (see Table S5). The experimental error of all peaks was determined to be ±1.54 s.

Wavenumber /cm^{-1}	Assignment	Time /s
2028	V=O overtone	29.1
1993	V=O overtone	30.2
1612	v_{as} propylene C=C	31.2
3739	Isolated anatase Ti-OH	31.2
1369	v_s formate O-C-O	32.2
1470	v_s carbonate O-C-O	33.3
3601	V-OH	35.4
3635	Isolated rutile Ti-OH	36.4

In-phase angle analysis shows that all time constants for P25+1.2 V/nm² are in a very similar range, especially when the experimental uncertainty is considered. The peaks at 2028, 1993, 1612 and 3739 cm^{-1} appear quite simultaneously as one group. This behavior is similar to that of VO$_x$/CeO$_2$, as the vanadyl peak and the Ti-OH species react first, indicating a fast transfer of hydrogen from propane to the titania surface and then to the vanadyl group. The Ti-OH species is a transient species mediating the hydrogen transfer, as determined from ME-DRIFTS (see Figure 7), while hydrogen binds more permanently to vanadia as these species can be observed in static operando experiments. The inverted reaction sequence, where the first hydrogen is rapidly transferred to rutile Ti-OH via vanadia with subsequent V-OH formation and concurrent olefin formation thereby seems unlikely, as this would necessitate the presence of a transient V-OH group at the beginning of the reaction sequence. As can be seen in Table 4, V-OH appears towards the end of the sequence, which supports the proposed reaction sequence where hydrogen is transferred from propane to vanadia via titania exclusively. Interestingly, the sequence of steps is inverted compared to VO$_x$/CeO$_2$ catalysts used for the same reaction, where the vanadyl peak mediated the hydrogen transfer from propane to the ceria surface.[7,8] This catalyst-dependent behavior can be explained by the different reducibilities, as the vanadia oxygen atoms are more reducible than titania, thereby delivering the oxygen necessary for the reaction, whereas on a ceria catalyst, ceria lattice oxygen is much more

reducible than vanadia.[72,73] Thus, the component that is more difficult to reduce is used as the transfer site, as the hydrogen is bound only loosely so that it can be readily transferred to the active oxygen component. This further shows that the oxygen atoms used for the hydrogen transfer are different than those used to facilitate the oxidation by formation of water. The additional peak at 1612 cm^{-1} is caused by the C=C vibration of the newly formed propylene, which indicates that propylene formation occurs directly after the initial hydrogen abstraction, consistent with a mechanism in which the first C-H abstraction is the rate-determining step and the remaining reaction steps follow directly afterwards.

After the initial hydrogen transfer and propylene formation, peaks at 1369 and 1470 cm^{-1} appear, which are attributed to formate and carbonate species, indicating that CO_x is formed on a similar time scale as propylene. This suggests that both propylene and CO_x are formed in parallel instead of CO_x being formed from propylene as a result of over-oxidation as the time difference between the C=C bond and the formate/carbonate is within the margin of error. However, a very fast over-oxidation of propylene to CO_x within the experimental error cannot be excluded. Subsequently, additional OH groups are detected, which are assigned to bridged OH and terminal OH groups on rutile. These may constitute a more stable state not facilitating further reaction and may be created by the dissociation of water produced during the reaction.[85–87] An additional peak is observed at ~1560 cm^{-1}, which can be assigned to different formate species, which are probably exclusive to the clean titania surface, as they show a significant presence on P25 but are only weakly present on the 0.1 V/nm² sample and absent on any of the samples with higher vanadia loading. For P25+0.5 V/nm², a similar temporal evolution is observed (see Figure S28 and Table S5), while P25, P25+0.1 V/nm² and P25+2.5 V/nm² deviate from the described behavior. Propane ODH over bare P25 follows a different reaction mechanism, which changes the determined time constants and P25+0.1 V/nm² shows a mixture of the reaction mechanisms over bare P25 and vanadia-loaded P25, explaining that the C=C double bond appears before the V=O signal, as some of the propane is converted earlier on the bare P25 surface. This is in line with all the previous observations, where the P25+0.1 V/nm² sample seems to represent an intermediate state between bare titania and vanadia-loaded titania, showing characteristics of both systems. The time constant of the V=O bond on the P25+2.5 V/nm² sample is shifted to much larger time values compared to the other vanadia-loaded samples, which agrees with the proposed

change in reaction mechanism when oligomers occur at this loading, where linear V-O-V bonds are the main active site providing the oxygen that drives the oxidation reaction. This further supports the change in reaction mechanism between the 1.2 and 2.5 V/nm² samples.

3.4. Isotopic Exchange Experiments

To confirm the previous assignments made for the structural dynamics during operando UV-Raman and transient IR spectroscopy, isotopic exchange experiments were performed (see Figure 9). Using $^{18}O_2$, these allow the oxygen transfer paths to be followed during UV-Raman spectroscopy, while the use of C_3D_8 can map the hydrogen transfer paths during ME-DRIFTS. Additionally, the influence of the isotopic exchange on the conversions was measured to obtain additional confirmation about the rate-determining step, which may in principle be due to either C-H bond breaking or catalyst reoxidation (see Figure 9d). The full PSD spectra for P25 and P25+1.2 V/nm² are shown in the SI (see Figure S31). For the exchange experiments, the samples were measured at 320 °C in different gas atmospheres, first under oxidizing conditions (12.5% O_2/He), then under reactive conditions (12.5% O_2/12.5% C_3H_8/He), and finally under reactive conditions with the isotopically labelled gas (12.5% $^{18}O_2(O_2)$/12.5% $C_3D_8(C_3H_8)$/He) to determine which changes are caused by the isotopically labelled gas.
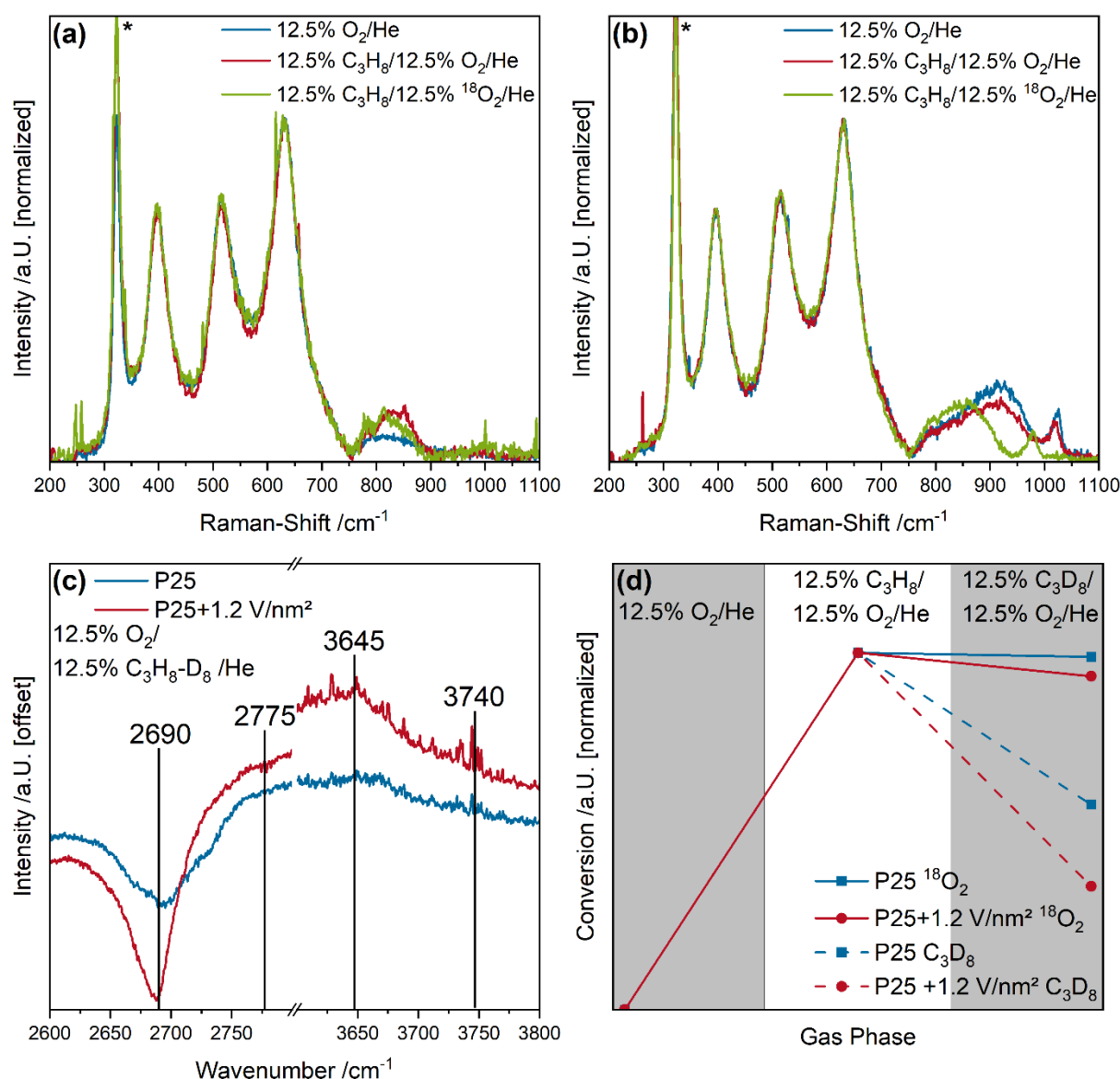
Figure 9: UV-Raman (385 nm excitation) spectra of **(a)** bare P25 and **(b)** P25+1.2 V/nm² measured under oxidizing (12.5% O_2/He), reactive (12.5% O_2/12.5% C_3H_8/He), and $^{18}O_2$ isotopically labelled reactive (12.5% $^{18}O_2$/12.5% C_3H_8/He) conditions. The spectra were normalized and the peak originating from the used CaF_2 window is marked with an asterisk. For comparison, ME-DRIFTS was recorded during isotopic exchange (constant oxygen and propane flow switched between h8-propane and d8-propane) and in **(c)** the resulting PSD spectra are shown, with the positions of the exchanged Ti-OH positions being highlighted. **(d)** Conversions were determined for operando experiments using $^{18}O_2$ and C_3D_8 to determine the kinetic isotopic effect. The full isotopically labelled PSD spectra of the samples are given in the SI (see Figure S31).

Bare P25 shows an increase in the rutile E_{2g} mode when switching from oxidative to reactive conditions, as discussed above (see Figure 4a). When switching to isotopically labelled $^{18}O_2$, a shift at the rutile E_{2g} mode at 820 cm^{-1} is detected,

indicating that the phase-transition between anatase and rutile is facilitated by an oxygen exchange with an affiliated reduction due to oxygen vacancy formation, confirming our proposal that the reaction occurs on a defective rutile/anatase interface. For the vanadia-loaded sample, we see a red-shift of the features at 920 and 1020 cm^{-1}, related to V-O-V and V=O bonds, respectively. Notably, the peaks at 820 and 860 cm^{-1} appear to be unchanged, indicating that neither the V-O-Ti interface nor the titania support itself are directly participating in the reaction, which confirms our previously proposed mechanism where only the vanadia-related oxygen atoms contribute to the overall propane conversion. In addition, the C_3H_8/C_3D_8 isotopic exchange experiment during ME-DRIFTS reveals that both Ti-OH groups at 3645 and 3740 cm^{-1} are present in the PSD spectra, indicating that they actively participate in the reaction. The full isotopic exchange ME-DRIFT spectra (see Figure S31) reveal that also formate species are detected during the experiment, indicating that they are an active species in the formation of CO_x, confirming the assignments, as only hydrogen-containing adsorbate peaks should be observable during isotopic exchange MES of h/d-propane.

The determined conversions during the isotopic exchange experiments show that the extent of the kinetic isotopic effect (KIE) depends on the isotopically labelled gas used. For the C_3H_8/C_3D_8 measurements, the KIE is 1.83 for bare P25 and 3.12 for P25+1.2 V/nm², which is in agreement with previously determined KIEs of hydrogen/deuterium exchange if the hydrogen bond is broken during the rate-determining step.[88] For comparison, the KIE of the $^{18}O_2/^{16}O_2$ isotopic exchange is 1.01 and 1.07 for bare P25 and P25+1.2 V/nm², respectively. Despite the lower mass difference between $^{18}O_2$ and $^{16}O_2$ in comparison to D_2 and H_2, the expected KIE for a reaction that uses molecular oxygen for the reoxidation as the rate-determining step would be much higher, at approximately 1.15.[89] The very low oxygen KIE for bare P25 might be caused by the fact that P25 is barely reduced during the reaction and the main reaction occurs from propane to carbon; little reoxidation is needed. Therefore, from the determined KIEs, we can conclude that the C-H bond breaking in propane is the rate-determining step, in agreement with our time constant results from MES. The TiO_2 support facilitates this bond breakage through Ti-OH formation, thus providing an explanation for the low activation energies and high reaction rates typically observed for VO_x/TiO_2 catalysts.[5]

3.5. Reaction Mechanism

In this section, we propose a reaction mechanism for propane ODH over VO_x/TiO_2 catalysts based on the results from multiple operando and transient spectroscopies. Firstly, the first C-H bond in propane is broken over titania surface lattice oxygen (Ti-O-Ti) (see Figure 9d) and one hydrogen is abstracted to the titania surface forming a singly-bound Ti-OH group on anatase (see Figure 7b). A bond breakage at the V-O-Ti interface appears unlikely since no changes of the V-O-Ti feature were observed in operando UV-Raman spectroscopy. The nature of the C-H bond breakage cannot be further specified. On one hand, no paramagnetic electrons were detected during previous operando EPR experiments,[34] which may suggest a heterolytic bond breakage. On the other hand, as the initial state is expected to be short-lived, it is likely to occur below the detection limit of the method. The hydrogen is then quickly transferred to the V-O-V bond of a doubly bridged dimeric species as interim storage for the hydrogen before the reduction of vanadia (see Figures 1, 4 and 5). Here, the transfer step of the proton and the electron required for the V-OH formation and reduction from V^{5+} to V^{4+} can either proceed sequentially or coupled (PCET). However, a further specification is not possible as it would require knowledge of the activation energy of the respective steps,[90] which is not available from the presented data. Possible electron donors may include reduced Ti^{3+} sites, which are formed during the reaction (see Figure 6). The transfer to the doubly bridged V-O-V oxygen instead of V=O is probably favored for the first hydrogen transfer from titania to vanadia during the selective conversion, which due to its worse reducibility decreases the likelihood of over-oxidation to CO_x.[10,11,13] Furthermore, the V-O-V structure is, due to the double bridge, not fully broken during this transfer, and therefore, the deflection from the equilibrium structure is comparably small. The transfer step may thus be kinetically favored compared to the direct transfer. Along these lines previous DFT calculations for VO_x/CeO_2 have shown that the direct and indirect transfer transition states had, within the margin of error, similar energies.[91] The proposed scenario is supported by our experimental findings (see Table 4 and Figure 7), as the spectroscopic data clearly presents a transient Ti-OH species that occurs first in the temporal evolution of adsorbates and is therefore linked to the initial C-H bond breakage. Hereby, the number of bridged V-O-V bonds in vanadia dimers seems to be important for the conversion of propane (see Figure 5c) as they are an important structure for the intermediate storage of hydrogen and show large structural changes (see Figure 4).

Nevertheless, besides dimers, also monomeric vanadia species are highly active during the reaction, based on the large increase in activity for the P25+0.1 V/nm² sample, and are likely to significantly contribute in parallel to the conversion at higher loadings. Since the V-O-V bond clearly participates in the reaction if it is available on the surface, we expect a mixture of active sites to be formed. Following the first hydrogen abstraction, the second hydrogen abstraction, also mediated by the titania surface, is transferred to a V=O bond, which is then used to facilitate propane ODH by its reduction together with the hydrogen stored at the V-O-V bond. The mechanism of this hydrogen transfer appears to be similar to the first one, as no additional intermediates are observed in PSD spectra on the timescale of the C=C bond formation (compare Figure 8 and Table 4). From the analysis of the rutile content and the previous literature, it seems that the amount of rutile dispersed in the catalytically more active anatase phase is crucial in increasing the degree of oligomerization of vanadia due to its higher mobility on the rutile surface. The higher degree of oligomerization leads to a higher concentration of dimeric species, that is, more V-O-V bonds, and therefore increases the reaction rate. The additional hydrogen atoms form a water molecule using a vanadyl oxygen atom, leaving the vanadium atom in a reduced state (see Figure 6c). At higher loadings (2.5 V/nm²), the first oligomeric species start to appear (see Figure 1, 2, and 5), which are likely to have more linear V-O-V bonds, and the active oxygen that is reduced in the reaction shifts from the V=O to the linearly bound V-O-V bond (see Figure 4c and 5c), indicating that it is likely to be more reducible than the V=O bonds that were previously used. The conversion via this V-O-V bond appears to be less selective than via the V=O bonds, which would be in agreement with its higher reducibility, as the P25+2.5 V/nm² sample shows a lower selectivity than the P25+1.2 V/nm² sample at the same conversion (see Figure 3), while also showing less V=O dynamics and more V-O-V dynamics (see Figure 4). This might be caused by the higher reducibility of linear V-O-V bonds formed in the oligomers at higher loadings compared to doubly bridged V-O-V or V=O atoms and demonstrates the strong dependence of the vanadia active site on its nuclearity. The reduced vanadium atom can then be re-oxidized by gas-phase oxygen, as the oxygen mobility in titania is too low to participate in the redox cycle.[18] The re-oxidation of vanadia is not rate-determining (see Figure 9d). A reaction mechanism where hydrogen is both stored and reduces the V-O-V or the V=O bond at which it is stored cannot be excluded due to the simultaneous dynamics of the two bonds (see Figure 4c) but seems to be less

likely due to the different reducibilities. During the entire selective oxidation process, propane does not seem to be directly adsorbed on the catalyst surface, as in neither static operando DRIFTS nor ME-DRIFTS could any propane-related adsorbates be detected, indicating a pure redox mechanism. For the formation of CO_x, multiple carbonate and formate adsorbates could be detected, indicating a change of the reaction mechanism to an associative mechanism during total oxidation. As these processes occur on a very similar time scale (see Figure 8b and Table 4), whether the propane is adsorbed seems to play an important role in determining whether it is selectively or totally oxidized, indicating a site-dependence in addition to the nuclearity dependence.

To close the catalytic cycle, the catalyst is regenerated by oxygen, which may happen in different ways. One possibility would be that starting from a dimeric V^{3+} site, which results from the oxidation of two propane molecules, adsorption of molecular oxygen first leads to the formation of a V-O-O-V bridge and then, after O-O bond breakage, to the formation of two V=O sites. Another possibility, which is also compatible with monomeric sites, might be coupled to the total oxidation reaction. Here, a V^{3+} site might adsorb an O_2 molecule, which results in a very reactive oxygen molecule that might react with additional propane towards the detected formate/ carbonate species, while regenerating the catalyst. This pathway could explain the limited reaction selectivity, besides the presence of bare TiO_2 facilitating total oxidation, and would also be in favor of the argument that total oxidation occurs in parallel to the selective oxidation. Therefore, depending on the vanadia nuclearity, a combination of both pathways seems likely.

In comparison, bare titania also shows the transient formation of Ti-OH groups (see Figure 7), but the abstracted hydrogen cannot be transferred to vanadia. As titania is much harder to reduce than vanadia, the conversions are lower due to reduced oxygen availability. When the selective oxidation takes place, lattice oxygen from the anatase/rutile interface is used for the oxidation, resulting in an increased amount of rutile (see Figure 4a) and an oxygen vacancy (see Figure 6c). Besides the selective oxidation, the main side product formed by the bare titania samples is carbon, which deposits on the catalyst surface and is likely to be caused by the high temperatures needed to activate titania lattice oxygen. This may result, for example, from propane adsorption at a site, where no anatase/rutile interface is present and therefore a higher defect formation energy is expected, which may lead to propane reaction to carbon.

The broad applicability of the results obtained in this study are demonstrated by the SBA-15-based $VO_x/TiO_2/SiO_2$ layered system, which was investigated in the same way as the P25 samples and is discussed in detail in the SI. Even though the titania structure (especially the phase composition between anatase, rutile and amorphous titania) is very different from P25, the structural dynamics are very similar to those of the P25 samples and can explain the reactivity behavior of this sample.

Based on the previous results and discussion a mechanistic scheme is proposed (see Figure 10) that summarizes the main processes during the selective oxidation of propane over VO_x/TiO_2, but additional processes can occur simultaneously to form CO_x at spots that are nuclearity- and site-dependent. The arrow from bridged V-O-V to Ti-OH in the first hydrogen transfer step of the mechanistic scheme indicates that the hydrogen bound to the titania surface is transferred to V-O-V and new hydrogen is transferred from propane to the titania surface via an additional Ti-OH instead of a direct transfer from propane to V-O-V. The asterisk (C_3H_6, C_3H_7) indicates that the exact geometry and interaction between the adsorbate molecule and the catalyst surface is not known, which is due to the fact that the adsorbate is short-lived (see Table 4). The catalytic cycle is closed by the regeneration by molecular oxygen as discussed above.
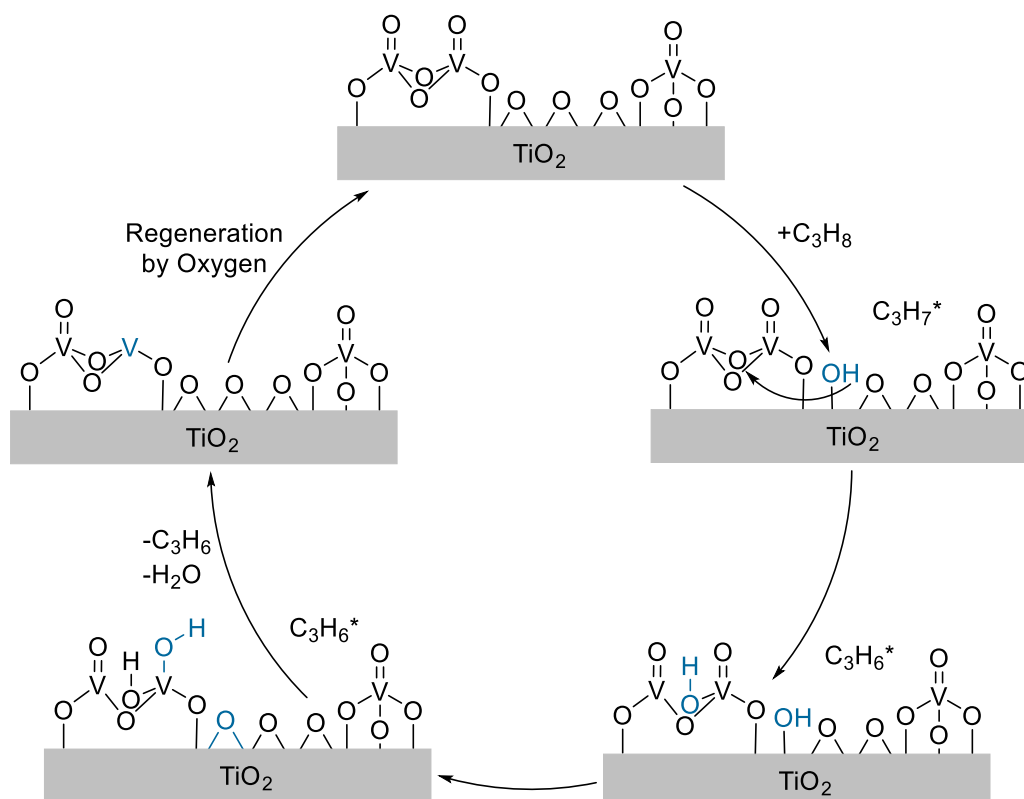
Figure 10: Proposed reaction mechanism for the ODH of propane over vanadia-loaded titania (P25) based on operando and transient spectroscopic analysis. Exemplarily, the reaction of one propane molecule over a dimer species is shown. Broken and newly formed bonds are marked in blue. For details see text.

4. Conclusion

In this work, we present a combination of extensive structural characterization, static operando, and transient spectroscopies, including multi-wavelength Raman, UV-Vis, ^{51}V ssNMR, XPS, XRD, and ME-DRIFT spectroscopy, to understand the structure and the reaction mechanism of propane ODH over VO_x/TiO_2 catalysts. To avoid typical problems of UV methods with self-absorption on highly UV absorbing TiO_2, we used multiple Raman wavelengths tuned to avoid most of the TiO_2 absorption, while still selectively enhancing the titania intensity through resonance effects. We also synthesized $VO_x/TiO_2/SiO_2$ samples in order to reduce the amount of bulk TiO_2 and to obtain more insights into its structure by decreasing its absorption even further. The ALD-synthesized samples can furthermore demonstrate the applicability of our results over a broader range of different types of titania. In combination with other spectroscopic methods, especially transient IR spectroscopy, we established an experimental basis to obtain a detailed mechanistic understanding of the propane ODH reaction.

By using the described set-up, we were able to answer the four key questions often debated in the literature for VO_x/TiO_2 systems for the propane ODH reaction, which were outlined in the introduction. First, the active sites could be identified by a combination of ^{51}V ssNMR and UV-Raman spectroscopy and was determined to be oxygen atoms of vanadia, where the oxygen atoms of dimeric species are preferred over oxygen atoms from monomeric sites. Second, the loading-dependence of the active site was determined by a nuclearity-dependent analysis of the vanadia structure and its reactivity. This type of analysis has proved to be difficult in the past for VO_x/TiO_2 systems, as the Ti:V contrast is much too low for electron microscopy and the vanadyl fine structure is not very defined using vibrational spectroscopy (unlike for VO_x/CeO_2). Combining ^{51}V ssNMR and UV-Raman spectroscopy, we were able to show that for P25 as a titania support, vanadia nuclearities could be determined and quantified using direct spectroscopic evidence. Hereby, the V=O oxygen was identified to be most active as the propane ODH facilitating oxygen atom as long as only doubly bridged V-O-V bonds from dimeric vanadia species were present at low loadings. When the loading was increased to a point where oligomeric species with linearly bridged oxygen

atoms started to form, they began to become more active due to their better reducibility, accompanied by a lower selectivity towards propylene.

Besides the structural changes in vanadia, the exact influence of titania on the catalysts´ activity was of debate. Possible influences could be (1) an active participation in the reaction of the titania by providing lattice oxygen to participate in the redox cycle, (2) the coordination of vanadia in comparison to other supports, lowering the activation barrier, or (3) both ways of titania participation happening simultaneously.[4–6] For propane ODH we were able to identify two ways in which titania influences the reaction. First, the amount of rutile dispersed in the anatase phase in the titania support can lead to different degrees of oligomerization of vanadia, and as the oligomerization degree is highly important and changes the active oxygen atom, it can thereby influence the activity significantly. The second way in which titania participates in the reaction was identified directly via spectroscopy for the first time using transient IR spectroscopy. Titania facilitates the first C-H bond breaking, which is the rate-determining step, via a very quick hydrogen transfer onto the titania surface, forming a Ti-OH group, only detectable using transient spectroscopy, followed by a hydrogen transfer onto the vanadia V=O or V-O-V bonds, depending on the nuclearity. Therefore, for propane ODH, titania enhances the activity by both directly participating in the reaction and coordinating the vanadia in a way that facilitates the reaction. Oxygen vacancies in the titania lattice could not be detected for vanadia-loaded samples, indicating that titania lattice oxygen is not actively participating during propane ODH.

Finally, the CO_x formation was determined to be a parallel reaction to propylene formation by transient IR spectroscopy and the decision whether selective or total oxidation occurs depends on whether propane adsorbs onto the catalyst or not, as carbonate and formate were the only adsorbates detectable in IR spectroscopy, indicating a site-dependence for both reaction pathways.

Based on our results, we were able to observe both the oxygen and hydrogen transfer paths on the catalyst and determine the influence of the titania support on both pathways, including the adsorbate dynamics on both the propylene and the CO_x pathways, as well as their influence on the selectivity. Combining all of the mechanistic information, we were able to propose a detailed mechanistic picture of the propane ODH reaction mechanism over VO_x/TiO_2 catalysts.

Our results demonstrate the potential of the combination of different operando spectroscopic methods with transient spectroscopy for elucidating the surface dynamics during ODH reactions over supported metal oxide systems. The approach can also be easily transferred to different materials and reactions, and, due to the widespread use of IR spectroscopy, the transient IR approach can readily be adopted to many different systems, performing detailed mechanistic analysis.

Declaration of Competing Interest

The authors declare that they have no known competing financial interests or personal relationships that could have appeared to influence the work reported in this paper.

Supporting Information

The supporting information contains additional technical information, and additional results from structural characterization, operando spectroscopic analysis, and transient DRIFTS.

Acknowledgements

References

(1) Amghizar, I.; Vandewalle, L. A.; van Geem, K. M.; Marin, G. B. New Trends in Olefin Production. *Engineering* **2017**, *3* (2), 171–178. DOI: 10.1016/j.eng.2017.02.006.

(2) Cavani, F.; Ballarini, N.; Cericola, A. Oxidative dehydrogenation of ethane and propane: How far from commercial implementation? *Catal. Today* **2007**, *127* (1-4), 113–131. DOI: 10.1016/j.cattod.2007.05.009.

(3) Carrero, C. A.; Schloegl, R.; Wachs, I. E.; Schomaecker, R. Critical Literature Review of the Kinetics for the Oxidative Dehydrogenation of Propane over Well-Defined Supported Vanadium Oxide Catalysts. *ACS Catal.* **2014**, *4* (10), 3357–3380. DOI: 10.1021/cs5003417.

(4) Chen, K.; Bell, A. T.; Iglesia, E. Kinetics and Mechanism of Oxidative Dehydrogenation of Propane on Vanadium, Molybdenum, and Tungsten Oxides. *J. Phys. Chem. B* **2000**, *104* (6), 1292–1299. DOI: 10.1021/jp9933875.

(5) Dinse, A.; Frank, B.; Hess, C.; Habel, D.; Schomäcker, R. Oxidative dehydrogenation of propane over low-loaded vanadia catalysts: Impact of the support material on kinetics and selectivity. *J. Mol. Catal. A: Chem.* **2008**, *289* (1-2), 28–37. DOI: 10.1016/j.molcata.2008.04.007.

(6) Beck, B.; Harth, M.; Hamilton, N. G.; Carrero, C.; Uhlrich, J. J.; Trunschke, A.; Shaikhutdinov, S.; Schubert, H.; Freund, H.-J.; Schlögl, R.; Sauer, J.; Schomäcker, R. Partial oxidation of ethanol on vanadia catalysts on supporting oxides with different redox properties compared to propane. *J. Catal.* **2012**, *296*, 120–131. DOI: 10.1016/j.jcat.2012.09.008.

(7) Schumacher, L.; Hess, C. The active role of the support in propane ODH over VO_x/CeO_2 catalysts studied using multiple operando spectroscopies. *J. Catal.* **2021**, *398* (13), 29–43. DOI: 10.1016/j.jcat.2021.04.006.

(8) Schumacher, L.; Weyel, J.; Hess, C. Unraveling the Active Vanadium Sites and Adsorbate Dynamics in VO_x/CeO_2 Oxidation Catalysts Using Transient IR Spectroscopy. *J. Am. Chem. Soc.* **2022**, *144* (32), 14874–14887. DOI: 10.1021/jacs.2c06303.

(9) Zaleska, A. Doped-TiO_2: A Review. *Recent Pat. Eng.* **2008**, *2* (3), 157–164. DOI: 10.2174/187221208786306289.

(10) Arnarson, L.; Falsig, H.; Rasmussen, S. B.; Lauritsen, J. V.; Moses, P. G. A complete reaction mechanism for standard and fast selective catalytic reduction of nitrogen oxides on low coverage VO_x/TiO_2(001) catalysts. *J. Catal.* **2017**, *346*, 188–197. DOI: 10.1016/j.jcat.2016.12.017.

(11) Kwon, D. W.; Park, K. H.; Hong, S. C. Influence of VO_x surface density and vanadyl species on the selective catalytic reduction of NO by NH_3 over VO_x/TiO_2 for superior catalytic activity. *Appl. Catal. A: Gen.* **2015**, *499*, 1–12. DOI: 10.1016/j.apcata.2015.04.005.

(12) Shen, J.; Hess, C. High Surface Area VO_x/TiO_2/SBA-15 Model Catalysts for Ammonia SCR Prepared by Atomic Layer Deposition. *Catalysts* **2020**, *10* (12), 1386. DOI: 10.3390/catal10121386.

(13) Won, J. M.; Kim, M. S.; Hong, S. C. Effect of vanadium surface density and structure in VO_x/TiO_2 on selective catalytic reduction by NH_3. *Korean J. Chem. Eng.* **2018**, *35* (12), 2365–2378. DOI: 10.1007/s11814-018-0158-x.

(14) Bertinchamps, F.; Treinen, M.; Blangenois, N.; Mariage, E.; Gaigneaux, E. Positive effect of NO on the performances of VO_x/TiO_2-based catalysts in the total oxidation abatement of chlorobenzene. *J. Catal.* **2005**, *230* (2), 493–498. DOI: 10.1016/j.jcat.2005.01.009.

(15) Bertinchamps, F.; Treinen, M.; Eloy, P.; Dos Santos, A.-M.; Mestdagh, M. M.; Gaigneaux, E. M. Understanding the activation mechanism induced by NO_x on the performances of VO_x/TiO_2 based catalysts in the total oxidation of chlorinated VOCs. *Appl. Catal. B: Environ.* **2007**, *70* (1-4), 360–369. DOI: 10.1016/j.apcatb.2005.11.022.

(16) Ghampson, I. T.; Pecchi, G.; Fierro, J.L.G.; Videla, A.; Escalona, N. Catalytic hydrodeoxygenation of anisole over Re-MoO_x/TiO_2 and Re-VO_x/TiO_2 catalysts. *Appl. Catal. B: Environ.* **2017**, *208*, 60–74. DOI: 10.1016/j.apcatb.2017.02.047.

(17) Liu, J.; Sun, Q.; Fu, Y.; Shen, J. Preparation and characterization of mesoporous VO_x-TiO_2 complex oxides for the selective oxidation of methanol to dimethoxymethane. *J. Colloid Interface Sci.* **2009**, *335* (2), 216–221. DOI: 10.1016/j.jcis.2009.03.027.

(18) Zabilska, A.; Clark, A. H.; Moskowitz, B. M.; Wachs, I. E.; Kakiuchi, Y.; Copéret, C.; Nachtegaal, M.; Kröcher, O.; Safonova, O. V. Redox Dynamics of Active VO_x Sites Promoted by TiO_x during Oxidative Dehydrogenation of Ethanol Detected by Operando Quick XAS. *J. Am. Chem. Soc. Au* **2022**, *2* (3), 762–776. DOI: 10.1021/jacsau.2c00027.

(19) Sannino, D.; Vaiano, V.; Ciambelli, P. Innovative structured VO_x/TiO_2 photocatalysts supported on phosphors for the selective photocatalytic oxidation of ethanol to acetaldehyde. *Catal. Today* **2013**, *205*, 159–167. DOI: 10.1016/j.cattod.2012.07.038.

(20) Ohtani, B. Titania Photocatalysis beyond Recombination: A Critical Review. *Catalysts* **2013**, *3* (4), 942–953. DOI: 10.3390/catal3040942.

(21) Ciambelli, P.; Lisi, L.; Ruoppolo, G.; Russo, G.; Volta, J. C. Oxidative dehydrogenation of ethane over vanadium and niobium oxides supported catalysts. In *3rd World Congress on Oxidation Catalaysis, Proceedings of the 3rd World Congress on Oxidation Catalysis*; Studies in Surface Science and Catalysis; Elsevier, 1997; pp 285–294. DOI: 10.1016/S0167-2991(97)80989-5.

(22) Martínez-Huerta, M. V.; Fierro, J.L.G.; Bañares, M. A. Monitoring the states of vanadium oxide during the transformation of TiO_2 anatase-to-rutile under reactive environments: H_2 reduction and oxidative dehydrogenation of ethane. *Catal. Commun.* **2009**, *11* (1), 15–19. DOI: 10.1016/j.catcom.2009.08.002.

(23) Khodakov, A.; Olthof, B.; Bell, A. T.; Iglesia, E. Structure and Catalytic Properties of Supported Vanadium Oxides: Support Effects on Oxidative Dehydrogenation Reactions. *J. Catal.* **1999**, *181* (2), 205–216. DOI: 10.1006/jcat.1998.2295.

(24) Heracleous, E.; Machli, M.; Lemonidou, A. A.; Vasalos, I. A. Oxidative dehydrogenation of ethane and propane over vanadia and molybdena supported catalysts. *J. Mol. Catal. A: Chem.* **2005**, *232* (1-2), 29–39. DOI: 10.1016/j.molcata.2005.01.027.

(25) Lemonidou, A.A.; Nalbandian, L.; Vasalos, I.A. Oxidative dehydrogenation of propane over vanadium oxide based catalysts. *Catal. Today* **2000**, *61* (1-4), 333–341. DOI: 10.1016/S0920-5861(00)00393-X.

(26) Martra, G.; Arena, F.; Coluccia, S.; Frusteri, F.; Parmaliana, A. Factors controlling the selectivity of V_2O_5 supported catalysts in the oxidative dehydrogenation of propane. *Catal. Today* **2000**, *63* (2-4), 197–207. DOI: 10.1016/S0920-5861(00)00460-0.

(27) Christodoulakis, A.; Machli, M.; Lemonidou, A. A.; Boghosian, S. Molecular structure and reactivity of vanadia-based catalysts for propane oxidative dehydrogenation studied by in situ Raman spectroscopy and catalytic activity measurements. *J. Catal.* **2004**, *222* (2), 293–306. DOI: 10.1016/j.jcat.2003.10.007.

(28) Shee, D.; Rao, T.; Deo, G. Kinetic parameter estimation for supported vanadium oxide catalysts for propane ODH reaction: Effect of loading and support. *Catal. Today* **2006**, *118* (3-4), 288–297. DOI: 10.1016/j.cattod.2006.07.017.

(29) Viparelli, P. Oxidative dehydrogenation of propane over vanadium and niobium oxides supported catalysts. *Appl. Catal. A: Gen.* **1999**, *184* (2), 291–301. DOI: 10.1016/S0926-860X(99)00104-0.

(30) Grzybowska, B.; Słoczyński, J.; Grabowski, R.; Samson, K.; Gressel, I.; Wcisło, K.; Gengembre, L.; Barbaux, Y. Effect of doping of TiO_2 support with altervalent ions on physicochemical and catalytic properties in oxidative dehydrogenation of propane of vanadia–titania catalysts. *Appl. Catal. A: Gen.* **2002**, *230* (1-2), 1–10. DOI: 10.1016/S0926-860X(01)00951-6.

(31) Nitsche, D.; Hess, C. Structure of Isolated Vanadia and Titania: A Deep UV Raman, UV–Vis, and IR Spectroscopic Study. *J. Phys. Chem. C* **2016**, *120* (2), 1025–1037. DOI: 10.1021/acs.jpcc.5b10317.

(32) Baron, M.; Abbott, H.; Bondarchuk, O.; Stacchiola, D.; Uhl, A.; Shaikhutdinov, S.; Freund, H.-J.; Popa, C.; Ganduglia-Pirovano, M. V.; Sauer, J. Resolving the Atomic Structure of Vanadia Monolayer Catalysts: Monomers, Trimers, and Oligomers on Ceria. *Angew. Chem. Int. Ed.* **2009**, *121* (43), 8150–8153. DOI: 10.1002/ange.200903085.

(33) Avdeev, V. I.; Zhidomirov, G. M. Modeling the active centers of V_2O_5/SiO_2 and V_2O_5/TiO_2 supported catalysts. DFT theoretical analysis of optical properties. *J. Struct. Chem.* **2005**, *46* (4), 577–590. DOI: 10.1007/s10947-006-0174-2.

(34) Brückner, A. Killing three birds with one stone--simultaneous operando EPR/UV-vis/Raman spectroscopy for monitoring catalytic reactions. *Chem. Commun.* **2005** (13), 1761–1763. DOI: 10.1039/b418790c.

(35) Weyel, J.; Ziemba, M.; Hess, C. Elucidating Active CO–Au Species on Au/CeO$_2$(111): A Combined Modulation Excitation DRIFTS and Density Functional Theory Study. *Top. Catal.* **2022**, *65* (7-8), 779–787. DOI: 10.1007/s11244-022-01599-1.

(36) Scheurell, K.; Hoppe, E.; Brzezinka, K.-W.; Kemnitz, E. Bulk and surface properties of highly dispersed VO$_x$/ZrO$_2$, VO$_x$/SiO$_2$ and VO$_x$/TiO$_2$/SiO$_2$ systems and their relevance for propane oxidation. *J. Mater. Chem.* **2004**, *14* (16), 2560. DOI: 10.1039/b402924k.

(37) Rogg, S.; Hess, C. CO$_2$ as a soft oxidant for propane oxidative dehydrogenation: A mechanistic study using operando UV Raman spectroscopy. *J. CO2 Util.* **2021**, *50*, 101604. DOI: 10.1016/j.jcou.2021.101604.

(38) Sobel, N.; Hess, C.; Lukas, M.; Spende, A.; Stühn, B.; Toimil-Molares, M. E.; Trautmann, C. Conformal SiO$_2$ coating of sub-100 nm diameter channels of polycarbonate etched ion-track channels by atomic layer deposition. *Beilstein J. Nanotechnol.* **2015**, *6*, 472–479. DOI: 10.3762/bjnano.6.48.

(39) Ruff, P.; Schumacher, L.; Rogg, S.; Hess, C. Atomic Layer Deposition-Assisted Synthesis of Embedded Vanadia Catalysts. *ACS Catal.* **2019**, *9* (7), 6349–6361. DOI: 10.1021/acscatal.9b01385.

(40) Spende, A.; Sobel, N.; Lukas, M.; Zierold, R.; Riedl, J. C.; Gura, L.; Schubert, I.; Moreno, J. M. M.; Nielsch, K.; Stühn, B.; Hess, C.; Trautmann, C.; Toimil-Molares, M. E. TiO$_2$, SiO$_2$, and Al$_2$O$_3$ coated nanopores and nanotubes produced by ALD in etched ion-track membranes for transport measurements. *Nanotechnology* **2015**, *26* (33), 335301. DOI: 10.1088/0957-4484/26/33/335301. Published Online: Jul. 30, 2015.

(41) Waleska, P. S.; Hess, C. Oligomerization of Supported Vanadia: Structural Insight Using Surface-Science Models with Chemical Complexity. *J. Phys. Chem. C* **2016**, *120* (33), 18510–18519. DOI: 10.1021/acs.jpcc.6b01672.

(42) Oliveira, M. de; Seeburg, D.; Weiß, J.; Wohlrab, S.; Buntkowsky, G.; Bentrup, U.; Gutmann, T. Structural characterization of vanadium environments in MCM-41

molecular sieve catalysts by solid state ^{51}V NMR. *Catal. Sci. Technol.* **2019**, *9* (21), 6180–6190. DOI: 10.1039/C9CY01410A.

(43) Fernandez, C.; Bodart, P.; Amoureux, J. P. Determination of ^{51}V quadrupole and chemical shift tensor orientations in V_2O_5 by analysis of magic-angle spinning nuclear magnetic resonance spectra. *Solid State Nucl. Magn. Reson.* **1994**, *3* (2), 79–91. DOI: 10.1016/0926-2040(94)90026-4.

(44) Ziemba, M.; Weyel, J.; Hess, C. Elucidating the mechanism of the reverse water–gas shift reaction over Au/CeO_2 catalysts using operando and transient spectroscopies. *Appl. Catal. B: Environ.* **2022**, *301*, 120825. DOI: 10.1016/j.apcatb.2021.120825.

(45) Baurecht, D.; Fringeli, U. P. Quantitative modulated excitation Fourier transform infrared spectroscopy. *Rev. Sci. Instrum.* **2001**, *72* (10), 3782–3792. DOI: 10.1063/1.1400152.

(46) Weyel, J. *Phase Sensitive Detection for Spectroscopy*; Zenodo, 2020.

(47) Lettieri, S.; Pavone, M.; Fioravanti, A.; Santamaria Amato, L.; Maddalena, P. Charge Carrier Processes and Optical Properties in TiO_2 and TiO_2-Based Heterojunction Photocatalysts: A Review. *Materials (Basel, Switz.)* **2021**, *14* (7). DOI: 10.3390/ma14071645.

(48) Glassford, K. M.; Chelikowsky, JR. Optical properties of titanium dioxide in the rutile structure. *Phys. Rev. B* **1992**, *45* (7), 3874–3877. DOI: 10.1103/physrevb.45.3874.

(49) Daude, N.; Gout, C.; Jouanin, C. Electronic band structure of titanium dioxide. *Phys. Rev. B* **1977**, *15* (6), 3229–3235. DOI: 10.1103/PhysRevB.15.3229.

(50) Tang, H.; Berger, H.; Schmid, P. E.; Lévy, F. Optical properties of anatase (TiO_2). *Solid State Commun.* **1994**, *92* (3), 267–271. DOI: 10.1016/0038-1098(94)90889-3.

(51) Hess, C.; Hoefelmeyer, J. D.; Tilley, T. D. Spectroscopic Characterization of Highly Dispersed Vanadia Supported on SBA-15. *J. Phys. Chem. B* **2004**, *108* (28), 9703–9709. DOI: 10.1021/jp037714r.

(52) Larrubia, M. A.; Busca, G. An ultraviolet–visible–near infrared study of the electronic structure of oxide-supported vanadia–tungsta and vanadia–molybdena. *Mater. Chem. Phys.* **2001**, *72* (3), 337–346. DOI: 10.1016/s0254-0584(01)00329-7.

(53) Choudhury, B.; Choudhury, A. Oxygen defect dependent variation of band gap, Urbach energy and luminescence property of anatase, anatase–rutile mixed phase and of rutile phases of TiO_2 nanoparticles. *Phys. E (Amsterdam, Neth.)* **2014**, *56*, 364–371. DOI: 10.1016/j.physe.2013.10.014.

(54) Landmann, M.; Rauls, E.; Schmidt, W. G. The electronic structure and optical response of rutile, anatase and brookite TiO_2. *J. Condens. Matter Phys.* **2012**, *24* (19), 195503. DOI: 10.1088/0953-8984/24/19/195503.

(55) Bonapasta, A.; Filippone, F.; Mattioli, G.; Alippi, P. Oxygen vacancies and OH species in rutile and anatase TiO_2 polymorphs. *Catal. Today* **2009**, *144* (1-2), 177–182. DOI: 10.1016/j.cattod.2009.01.047.

(56) Bhattacharyya, K.; Varma, S.; Tripathi, A. K.; Bharadwaj, S. R.; Tyagi, A. K. Effect of Vanadia Doping and Its Oxidation State on the Photocatalytic Activity of TiO_2 for Gas-Phase Oxidation of Ethene. *J. Phys. Chem. C* **2008**, *112* (48), 19102–19112. DOI: 10.1021/jp807860y.

(57) Nagaveni, K.; Hegde, M. S.; Madras, G. Structure and Photocatalytic Activity of $Ti_{1-x}M_xO_{2\pm\delta}$ (M=W, V, Ce, Zr, Fe, and Cu) Synthesized by Solution Combustion Method. *J. Phys. Chem. B* **2004**, *108* (52), 20204–20212. DOI: 10.1021/jp047917v.

(58) Jiang, X.; Manawan, M.; Feng, T.; Qian, R.; Zhao, T.; Zhou, G.; Kong, F.; Wang, Q.; Dai, S.; Pan, J. H. Anatase and rutile in evonik aeroxide P25: Heterojunctioned or individual nanoparticles? *Catal. Today* **2018**, *300*, 12–17. DOI: 10.1016/j.cattod.2017.06.010.

(59) Burcham, L. J. In situ IR, Raman, UV-Vis DRS spectroscopy of supported vanadium oxide catalysts during methanol oxidation. *Top. Catal.* **2000**, *11/12* (1/4), 85–100. DOI: 10.1023/A:1027275225668.

(60) Balachandran, U.; Eror, N. G. Raman spectra of titanium dioxide. *J. Solid State Chem.* **1982**, *42* (3), 276–282. DOI: 10.1016/0022-4596(82)90006-8.

(61) Kryukova, G. N.; Zenkovets, G. A.; Mestl, G.; Schlögl, R. Structural study of titanium doped vanadia and vanadium doped titania catalysts. *React. Kinet. Catal. Lett.* **2003**, *80* (1), 161–169. DOI: 10.1023/A:1026000829726.

(62) Xie, S.; Iglesia, E.; Bell, A. T. Effects of Hydration and Dehydration on the Structure of Silica-Supported Vanadia Species. *Langmuir* **2000**, *16* (18), 7162–7167. DOI: 10.1021/la0003342.

(63) Hess, C.; Tzolova-Müller, G.; Herbert, R. The Influence of Water on the Dispersion of Vanadia Supported on Silica SBA-15: A Combined XPS and Raman Study. *J. Phys. Chem. C* **2007**, *111* (26), 9471–9479. DOI: 10.1021/jp0713920.

(64) Centi, G. Nature of active layer in vanadium oxide supported on titanium oxide and control of its reactivity in the selective oxidation and ammoxidation of alkylaromatics. *Appl. Catal. A: Gen.* **1996**, *147* (2), 267–298. DOI: 10.1016/s0926-860x(96)00179-2.

(65) Sanati, M.; Andersson, A. Ammoxtoation of toluene over TiO_2(B)-supported vanadium oxide catalysts. *J. Mol. Catal.* **1990**, *59* (2), 233–255. DOI: 10.1016/0304-5102(90)85055-m.

(66) Wachs, I. E. Raman and IR studies of surface metal oxide species on oxide supports: Supported metal oxide catalysts. *Catal. Today* **1996**, *27* (3-4), 437–455. DOI: 10.1016/0920-5861(95)00203-0.

(67) Lian, Z.; Deng, H.; Xin, S.; Shan, W.; Wang, Q.; Xu, J.; He, H. Significant promotion effect of the rutile phase on V_2O_5/TiO_2 catalysts for NH_3-SCR. *Chem. Commun.* **2021**, *57* (3), 355–358. DOI: 10.1039/d0cc05938b.

(68) Arena, F.; Frusteri, F.; Parmaliana, A. How oxide carriers affect the reactivity of V_2O_5 catalysts in the oxidative dehydrogenation of propane. *Catal. Lett.* **1999**, *60* (1/2), 59–63. DOI: 10.1023/A:1019074016773.

(69) Schwan, J.; Ulrich, S.; Batori, V.; Ehrhardt, H.; Silva, S. R. P. Raman spectroscopy on amorphous carbon films. *J. Appl. Phys.* **1996**, *80* (1), 440–447. DOI: 10.1063/1.362745.

(70) Sadezky, A.; Muckenhuber, H.; Grothe, H.; Niessner, R.; Pöschl, U. Raman microspectroscopy of soot and related carbonaceous materials: Spectral analysis and

structural information. *Carbon* **2005**, *43* (8), 1731–1742. DOI: 10.1016/j.carbon.2005.02.018.

(71) Silva, S. R. P.; Amaratunga, G. A. J.; Salje, E. K. H.; Knowles, K. M. Evidence of hexagonal diamond in plasma-deposited carbon films. *J. Mater. Sci.* **1994**, *29* (19), 4962–4966. DOI: 10.1007/BF01151085.

(72) Dutta, G.; Waghmare, U. V.; Baidya, T.; Hegde, M. S.; Priolkar, K. R.; Sarode, P. R. Origin of Enhanced Reducibility/Oxygen Storage Capacity of $Ce_{1-x}Ti_xO_2$ Compared to CeO_2 or TiO_2. *Chem. Mater.* **2006**, *18* (14), 3249–3256. DOI: 10.1021/cm060267i.

(73) Watanabe, S.; Ma, X.; Song, C. Characterization of Structural and Surface Properties of Nanocrystalline TiO_2-CeO_2 Mixed Oxides by XRD, XPS, TPR, and TPD. *J. Phys. Chem. C* **2009**, *113* (32), 14249–14257. DOI: 10.1021/jp8110309.

(74) Jaegers, N. R.; Lai, J.-K.; He, Y.; Walter, E.; Dixon, D. A.; Vasiliu, M.; Chen, Y.; Wang, C.; Hu, M. Y.; Mueller, K. T.; Wachs, I. E.; Wang, Y.; Hu, J. Z. Mechanism by which Tungsten Oxide Promotes the Activity of Supported V_2O_5/TiO_2 Catalysts for NO_x Abatement: Structural Effects Revealed by [51]V MAS NMR Spectroscopy. *Angew. Chem. Int. Ed.* **2019**, *58* (36), 12609–12616. DOI: 10.1002/anie.201904503.

(75) Hu, J. Z.; Xu, S.; Li, W.-Z.; Hu, M. Y.; Deng, X.; Dixon, D. A.; Vasiliu, M.; Craciun, R.; Wang, Y.; Bao, X.; Peden, C. H. F. Investigation of the Structure and Active Sites of TiO_2 Nanorod Supported VO_x Catalysts by High-Field and Fast-Spinning [51]V MAS NMR. *ACS Catal.* **2015**, *5* (7), 3945–3952. DOI: 10.1021/acscatal.5b00286.

(76) Jehng, J.-M.; Deo, G.; Weckhuysen, B. M.; Wachs, I. E. Effect of water vapor on the molecular structures of supported vanadium oxide catalysts at elevated temperatures. *J. Mol. Catal. A: Chem.* **1996**, *110* (1), 41–54. DOI: 10.1016/1381-1169(96)00061-1.

(77) Walter, A.; Herbert, R.; Hess, C.; Ressler, T. Structural characterization of vanadium oxide catalysts supported on nanostructured silica SBA-15 using X-ray absorption spectroscopy. *Chem. Cent. J.* **2010**, *4*, 3. DOI: 10.1186/1752-153X-4-3.

(78) van der Voort, P.; White, M. G.; Mitchell, M. B.; Verberckmoes, A. A.; Vansant, E. F. The effect of water on the structure of supported vanadium oxide structures. An FT-Raman, in situ DRIFT and in situ UV-VIS diffuse reflectance study. *Spectrochim. Acta Part A* **1997**, *53* (12), 2181–2187. DOI: 10.1016/S1386-1425(97)00145-5.

(79) Lamoureux, B.; Singh, V. R.; Jovic, V.; Kuyyalil, J.; Su, T.-Y.; Smith, K. E. Structural and electronic properties of thermally evaporated V_2O_5 epitaxial thin films. *Thin Solid Films* **2016**, *615*, 409–414. DOI: 10.1016/j.tsf.2016.07.062.

(80) Kuriechen, S. K.; Murugesan, S.; Paul Raj, S. Mineralization of Azo Dye Using Combined Photo-Fenton and Photocatalytic Processes under Visible Light. *J. Catalysis* **2013**, *2013* (4), 1–6. DOI: 10.1155/2013/104019.

(81) Yang, J.; Bai, H.; Tan, X.; Lian, J. IR and XPS investigation of visible-light photocatalysis—Nitrogen–carbon-doped TiO_2 film. *Appl. Surf. Sci.* **2006**, *253* (4), 1988–1994. DOI: 10.1016/j.apsusc.2006.03.078.

(82) Cano-Casanova, L.; Mei, B.; Mul, G.; Lillo-Ródenas, M. Á.; Román-Martínez, M. D. C. Photocatalytic Oxidation of Propane Using Hydrothermally Prepared Anatase-Brookite-Rutile TiO_2 Samples. An In Situ DRIFTS Study. *Nanomaterials* **2020**, *10* (7), 13–14. DOI: 10.3390/nano10071314.

(83) Hu, Z.; Wang, Z.; Guo, Y.; Wang, L.; Guo, L.; Zhang, J.; Zhan, W. Total Oxidation of Propane over a Ru/CeO_2 Catalyst at Low Temperature. *Environ. Sci. Technol.* **2018**, *16* (52), 9531–9541. DOI: 10.1021/acs.est.8b03448.

(84) Hadjiivanov, K. I.; Klissurski, D. G. Surface chemistry of titania (anatase) and titania-supported catalysts. *Chem. Soc. Rev.* **1996**, *25* (1), 61. DOI: 10.1039/cs9962500061.

(85) Mathieu, M. V.; Primet, M.; Pichat, P. Infrared study of the surface of titanium dioxides. II. Acidic and basic properties. *J. Phys. Chem.* **1971**, *75* (9), 1221–1226. DOI: 10.1021/j100679a008.

(86) Primet, M.; Pichat, P.; Mathieu, M. V. Infrared study of the surface of titanium dioxides. I. Hydroxyl groups. *J. Phys. Chem.* **1971**, *75* (9), 1216–1220. DOI: 10.1021/j100679a007.

(87) Tanaka, K.; White, J. M. Characterization of species adsorbed on oxidized and reduced anatase. *J. Phys. Chem.* **1982**, *86* (24), 4708–4714. DOI: 10.1021/j100221a014.

(88) Sharp, T. E.; Johnston, H. S. Hydrogen—Deuterium Kinetic Isotope Effect, an Experimental and Theoretical Study over a Wide Range of Temperature. *J. Chem. Phys.* **1962**, *37* (7), 1541–1553. DOI: 10.1063/1.1733321.

(89) Monnier, J. R.; Medlin, J.W.; Barteau, M.A. Use of Oxygen-18 to Determine Kinetics of Butadiene Epoxidation over Cs-Promoted, Ag Catalysts. *J. Catal.* **2001**, *203* (2), 362–368. DOI: 10.1006/jcat.2001.3358.

(90) Weinberg, D. R.; Gagliardi, C. J.; Hull, J. F.; Murphy, C. F.; Kent, C. A.; Westlake, B. C.; Paul, A.; Ess, D. H.; McCafferty, D. G.; Meyer, T. J. Proton-coupled electron transfer. *Chem. Rev.* **2012**, *112* (7), 4016–4093. DOI: 10.1021/cr200177j. Published Online: Jun. 18, 2012.

(91) Huang, C.; Wang, Z.-Q.; Gong, X.-Q. Activity and selectivity of propane oxidative dehydrogenation over VO_3/CeO_2(111) catalysts: A density functional theory study. *Chin. J. Catal.* **2018**, *39* (9), 1520–1526. DOI: 10.1016/S1872-2067(18)63072-4.